A METAPOPULATION MODEL FOR SYLVATIC *T. CRUZI* TRANSMISSION WITH VECTOR MIGRATION

Britnee Crawford

Dallas Baptist University
3000 Mountain Creek Pkwy
Dallas, TX 75211, USA

Christopher Kribs-Zaleta

UT Arlington Mathematics Dept
Box 19408
Arlington, TX 76019-0408, USA

(Communicated by James Watmough)

Abstract. This study presents a metapopulation model for the sylvatic transmission of *Trypanosoma cruzi*, the etiological agent of Chagas' disease, across multiple geographical regions and multiple overlapping host-vector transmission cycles. Classical qualitative analysis of the model and several submodels focuses on the parasite's basic reproductive number, illustrating how vector migration across patches and multiple transmission routes to hosts (including vertical transmission) determine the infection's persistence in each cycle. Numerical results focus on trends in endemic [equilibrium] persistence levels as functions of vector migration rates, and highlight the significance of the different epidemiological characteristics of transmission in each of the three regions.

1. **Introduction.** A vector-borne disease of major concern in the Americas, transmitted via insect vectors from the subfamily Triatominae, is Chagas' disease. Chagas' disease, discovered in 1909, is widespread in Mexico, Central America, and throughout Latin America. An estimated 8 to 11 million people are currently infected, with many unaware of their infection [57]. However, in the United States, fewer than 10 cases of autochthonous transmission have been reported [6]. Although more attention is being given to Chagas', incidence of the disease remains underreported, and Chagas' is classified as a neglected parasitic infection in the United States [11].

Although there have been few human cases in the U.S., the disease remains endemic in sylvatic cycles throughout Mexico and the United States. Sylvatic transmission cycles are vector-host cycles that occur naturally in the wild. In the United States, triatomine vectors are found in 26 states [30], involving approximately 11 triatomine vector species (with 8 of the 11 in Texas) and over 100 mammalian species. In the United States, some of the most common sylvatic hosts include opossums (*Didelphis virginiana*) and raccoons (*Procyon lotor*) in the southeastern parts of the country and woodrats (*Neotoma micropus*) in Texas (extending also into northern

---

parts of Mexico). Other species, such as dogs, armadillos, and skunks, and chickens have also been noted as relevant species in sylvatic settings (with canines part of some domestic and peridomestic cycles [10, 59]). Of the 11 vector species and mammalian species listed here, we identify two primary vector species associated with these hosts in the southeastern U.S., *Triatoma sanguisuga*, found all along the southeastern Atlantic coast from Florida into central Texas, and *Triatoma gerstaeckeri*, found mostly from central Texas south into states in northern Mexico [26]. In addition to the complex vector-host cycles, there are also multiple strains of *T. cruzi* circulating in these populations. There are 6 known strain types of *T. cruzi*, types I-VI, of which types I and IV are circulating in the United States. There are distinct differences between the strains, from host specificity to virulence. *T. cruzi* I, associated with Chagas' disease, is the primary strain circulating in Mexico (also found in hosts in the U.S.), while type IV is almost exclusively found in the United States [45].

Recent work by Crawford and Kribs-Zaleta [15] provides an understanding of how local vector dispersal can be described in terms of global effects, so that we may now consider a model that describes sylvatic cycles of *T. cruzi* over a large geographic area. Because *T. cruzi* is maintained in sylvatic cycles, we recognize the need to study the spatial spread of the disease, especially in North America, where risk of Chagas has only recently been studied [26, 23]. Here we investigate several models of *T. cruzi*, incorporating multiple modes of transmission and multiple patches. More specifically, we wish to focus our efforts on the effects of vector migration on sylvatic *T. cruzi* strain type IV transmission in two different North American host-vector cycles.

To date, the majority of mathematical models for Chagas disease have been studied in humans and vectors, rather than the animal hosts. Velasco-Hernández [54] modeled Chagas in humans using a model structure similar to the Ross-Macdonald malaria model [46, 33], but included another infectious compartment for chronically ill humans. Since infection with *T. cruzi* is maintained in reservoir (sylvatic) hosts and human transmission cycles cannot be sustained without them [21], recently more attention has been given to the spread of the *T. cruzi* parasite in *Triatoma* vectors and associated animal hosts [29, 27]. In each model, Kribs-Zaleta uses a deterministic SI model with one host and one vector to study the effects of alternative transmission modes for *T. cruzi*, namely vector consumption by animal hosts and vertical transmission in hosts. Results show that vertical transmission is not enough to maintain the infection cycle alone, but vertical transmission along with even an inefficient host-vector transmission cycle can sustain the *T. cruzi* infection cycle. Due to the nature of transmission of vector-borne disease, in which vectors and hosts (especially in sylvatic settings) may be easily affected by weather (mainly temperature and humidity) and landscape, spatial spread is a key element in studying a vector-borne disease.

Spatial spread of a disease can be modeled using continuous or discrete space. The majority of mathematical models involving the spatial spread of infectious diseases in continuous time and space are modeled using reaction-diffusion systems taking the form of a system of partial differential equations. Some studies incorporating spatial spread are the spread of rabies in the fox population [39], and the vector borne diseases dengue [34] and West Nile virus [32]. The results of such systems are generally described using traveling waves which describe the process of the spread of the disease, most often over a homogeneous landscape. In each model,

movement of either hosts or vectors (or both) is considered, with the underlying assumption that the movement is random.

Other types of models incorporating spatial spread include multi-patch metapopulation models in which movement occurs between n patches. Several models have been studied, including a multi-species model by Arino et al. [4], in which analytical results are given for several multi-species, multi-patch models. In the study, a formula is derived for the basic reproductive number R_0 for multiple species and multiple patches and global stability for the disease-free equilibrium is established for $R_0 < 1$. Allen et al. [3] gives a 3-patch model of hantavirus spread in reservoir and spillover species in which the outer patches represent the preferred habitat of the reservoir and spillover species and the middle patch represents the boundary region in which the species overlap. We note here that the overlap region was temporally- and spatially-dependent. The movement here is described in terms of number of visits per year to the boundary region and length of time spent there. Reproductive numbers for each patch were calculated, and it was determined that the greater number of interactions among species caused the reproductive number of the overlap patch to exceed the reproductive numbers of the patches representing preferred habitat, thereby causing a greater possibility of disease persistence.

In this study we consider three different geographical areas we refer to as patches. Each patch is described by a distinct transmission cycle between the hosts and vectors in the model. Patch 1 is defined by the *T. gerstaeckeri*-woodrat infection cycle in northern Mexico and southern Texas. Patch 3 is the south-eastern United States, including parts of Texas, Louisiana, Mississippi, Alabama, Georgia, and portions of the Carolinas and Florida panhandle and is defined by the *T. sanguisuga*-raccoon infection cycle, while patch 2 includes the south to southwest parts of Texas and a part of Coahuila, Mexico where we consider both species of vector and host to overlap. We assume the communication between patches and between cycles in patch 2 occurs through the movement of *Triatoma* vectors. *T. sanguisuga* migrates between patches 2 and 3, and between raccoons and woodrats in patch 2, while *T. gerstaeckeri* migrates between patches 1 and 2. We wish to investigate how increased vector migration affects prevalence in the overlap patch compared to the single-cycle patches.

In this study we develop and analyze an *S-I* metapopulation model with the aforementioned hosts and vectors, in which hosts may exhibit vertical transmission and vectors migrate between patches. We carry out standard analysis techniques, such as calculating R_0 for various sub-models of the larger metapopulation model as well as determining existence of endemic equilibria analytically (when tractable) in order to see effects of vector migration on R_0. Finally, we perform numerical analysis on the full model to determine effects of migration on prevalence of *T. cruzi*.

2. Problem formulation and model.

2.1. Problem statement and assumptions.
To establish stable large-scale demographics for hosts and vectors, we assume that the growth for each species will be logistic, and neither the hosts nor vectors identified in the model exhibit disease-induced mortality. Studies have shown that the *T. cruzi* infecting raccoons and opossums in areas in the south-southeastern U.S. are not pathogenic, and do not appear to cause any symptoms of Chagas to the usual host [40, 58].

Although triatomine bugs feed on many hosts in the wild, we consider woodrats and raccoons based on data that correlates their geographic location very closely with the vectors [41, 10, 42, 25]. In literature reviewed here, we have found the only host associated with *T. gerstaeckeri* is the southern plains woodrat [26, 18]. Therefore, we consider that the southern plains woodrat is the preferred host for the vector *T. gerstaeckeri*.

In this model there are several infection rates to be considered. We first distinguish between types of transmission routes. In this study, we consider both horizontal and vertical transmission routes, and we mention here that we group both stercorarian transmission and oral (host predation on infected vectors) transmission into a single horizontal transmission parameter. The infection rates may differ from vector to host and host to vector as well as by patch (geographical region). Biologically, the rate of infection between the hosts and vectors in each patch should be different. However, as seen in section 4 when calculating numerical estimates for the infection rate parameters (using a procedure called back-calculation), it is mathematically necessary to keep some of the rates the same. Thus, we assume that the rate of infection from raccoons to *T. sanguisuga* is the same in patches 2 and 3 and the rate of infection from *T. gerstaeckeri* to woodrats is the same in patches 1 and 2.

Literature suggests that *T. sanguisuga* will feed on other hosts besides raccoons, namely woodrats [18]. Thus, in patch 2, *T. sanguisuga* feeds on raccoons and woodrats. Some proportion of vector-woodrat contacts are made with *T. sanguisuga*, thus we define q_W as the proportion of vector-woodrat contacts made with *T. sanguisuga*, while $1 - q_W$ is the proportion made with *T. gerstaeckeri*. Furthermore, since *T. sanguisuga* feeds on both hosts, we define q_S as the proportion of *T. sanguisuga* contacts made with raccoons, while $1 - q_S$ is the proportion made with woodrats. We denote the per vector infection rate from *T. sanguisuga* to woodrats as β_{SW} and the per vector infection rate from woodrats to *T. sanguisuga* to be β_{WS}.

T. cruzi has been confirmed to be transmitted vertically among mice in laboratory conditions [38]. However, there is limited data on vertical transmission of *T. cruzi* in sylvatic hosts. We will assume that *T. cruzi* can be transmitted vertically in raccoons and woodrats.

Infection contact rates could be limited by the host or vector population. For our model, we assume that the limiting factor for infection from host to vector will be the vector population. The hosts are plentiful enough for vectors to feed as much as desired. Therefore, the vector population density will be the driving force in determining the infection rate, and the contact process saturates more quickly in the vector population than in the hosts. Thus, we consider the infection term from host to vector in the model to be based on several factors. Using similar derivation as in [28], we define the per-vector biting rate as z (in units of contacts per vector per time), and thus the total vector-feeding contact rate as $z \cdot N_v$ (with units of bites/time). Thus, to calculate the rate of new vector infections, we multiply the total vector-feeding contact rate by the proportion of contacts that involve uninfected vectors and infected hosts, multiplied by the proportion of contacts that result in an infection (π_v) (units of infected vectors/bite) obtaining

$$zN_v \cdot \frac{S_v}{N_v} \cdot \frac{I_h}{N_h} \cdot \pi_v = (\pi_v z)\frac{I_h}{N_h}S_v.$$

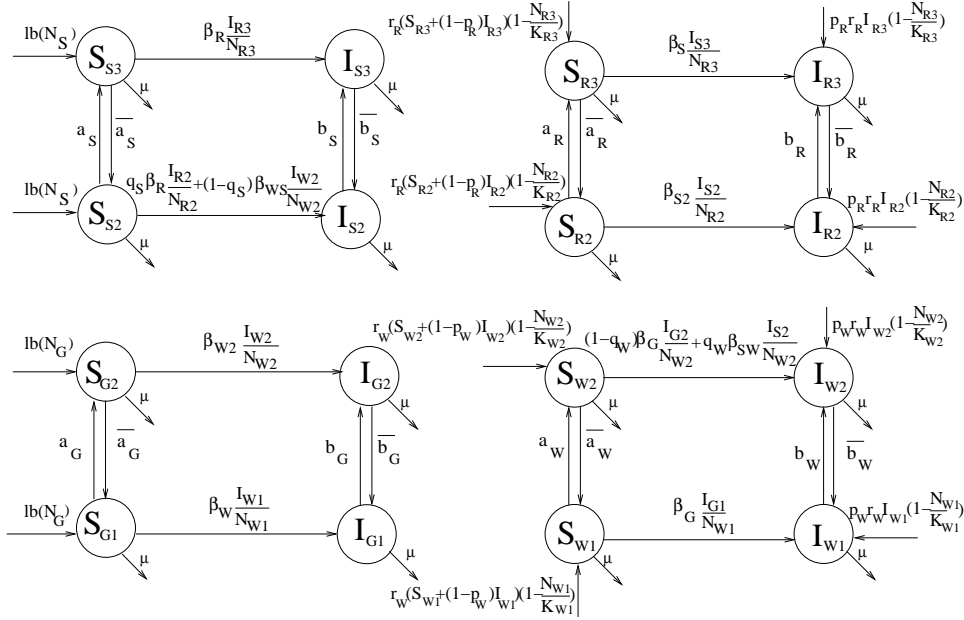To simplify, we write $\beta_h = \pi_v z$ (in units of 1/time).

FIGURE 1. Model (1). The migration rates represent outgoing rates which must be adjusted by the patch area ratios for incoming rates (see system (1))

We also need to describe the rate at which vectors infect hosts. Again, assuming that the vector to host infection will be limited by the vector population (vectors feeding as frequently as desired), we multiply the total vector-feeding contact rate by the proportion of contacts involving uninfected hosts and infected vectors, multiplied by the proportion of contacts resulting in an infection (with units infected hosts/bite),

$$zN_v \cdot \frac{S_h}{N_h} \cdot \frac{I_v}{N_v} \cdot \pi_h = (\pi_h z)\frac{I_v}{N_h}S_h.$$

In a similar manner, we define $\beta_v = \pi_h z$. But, we note here that β_v is not in units of 1/time, but rather infected hosts per vector per time. We will apply this assumption to the infection terms in the model using the appropriate vector and host subscripts.

2.2. **The model.** The model presented here is an *S-I* model incorporating migration and vertical transmission.

For each species we will use the general logistic birth rate $b(N) = rN\left(1 - \frac{N}{K}\right)$, where r represents the intrinsic population growth rate, N represents the total population density, and K is the carrying capacity of the population density. We will use this term for each vector and host population using the appropriate subscripts. The logistic birth rate gives a reasonable description of the drop-off in births as population density increases. With respect to the vector population, as intraspecific competition for hosts intensifies, females lay fewer eggs, and the eggs' hatch rate also decreases. We further mention that the hosts in the model exhibit vertical transmission. Therefore, we incorporate this into the model by defining the following functions: $f(N, I)$ and $g(N, I)$ represent the birth rates for the hosts exhibiting

vertical transmission. If only a proportion p $(0 < p < 1)$ of infected hosts transmit vertically, then $g(N, I) = pI \cdot r \left(1 - \frac{N}{K}\right)$, where p is the proportion of the offspring of infected hosts born infected with *T. cruzi*. Thus $f(N, I) = (S + (1-p)I) \cdot r \left(1 - \frac{N}{K}\right)$. We will apply this assumption to both hosts in the model, applying the appropriate subscripts. The natural per host and per vector mortality rates are denoted by μ_R, μ_W, μ_S, and μ_G. We distinguish clearly between the logistic birth and linear mortality rate because mortality is assumed to be spread evenly among infected and uninfected vectors and hosts, while births are assumed to contribute only to the susceptible class, except for vertical transmission described previously.

In this model we will assume linear migration based on the idea of local dispersion. We note that there are several different migration rates considered. We assume that hosts and vectors move at different rates, and those rates differ by species, by infection status, and by direction of migration. The migration parameters in the model are denoted by b_i or $\bar{b}_i$ for vectors and a_i or $\bar{a}_i$ for hosts, designating difference in direction of migration. Each subscript, i, is used to designate the migrating species, R, S, G, or, W. For example, $\bar{b}_G$ represents the migration rate of *T. gerstaeckeri* from patch 1 to 2, while b_G is the rate of *T. gerstaeckeri* from patch 2 to 1.

Furthermore, we note here that each patch has a different area, and the migration rates derived in [15] are affected by the size of the patch from which migration originates. In the metapopulation model described here, each differential equation represents the change in population density over time, thus the size of patch must also affect the population density of the vectors and hosts in each patch. Since we are considering migration of vectors between patches, the differences in population densities must be accounted for. For example, in order to account for the differing patch sizes, we consider the equation for the absolute number of infected *T. sanguisuga* vectors in patch 3, where A_3 denotes the area (in m^2) of patch 3 and the state variables have units of density. Then, the absolute number of vectors in patch 3 is given by

$$(I_{S3} A_3)' = \beta_R \frac{I_{R3}}{N_{R3}} S_{S3} A_3 - (\mu_S + b_S) I_{S3} A_3 + \bar{b}_S I_{S2} A_2.$$

It follows that

$$I'_{S3} = \beta_R \frac{I_{R3}}{N_{R3}} S_{S3} - (\mu_S + b_S) I_{S3} + \bar{b}_S \frac{A_2}{A_3} I_{S2}.$$

In the model, we write $\bar{b}_S \frac{A_2}{A_3} = \tilde{b}_S$ and $b_S \frac{A_3}{A_2} = \hat{b}_S$. This notation will be used more generally for northward and southward migration rates, respectively.

Finally, we make the following assumptions about the demographic and migration rates. First, for a given species (whether host or vector), in order for the population not to go extinct in a given patch, we must have $r > \mu + b$ (where b is the total per capita migration rate out of the patch)—that is, combined mortality and emigration cannot exceed the maximum growth rate. This seems biologically reasonable since no local vector or host extinction has been reported. Second, we further assume that $\mu > b$; this assumption can be justified by rewriting it as $1/b > 1/\mu$—that is, the average time before migrating exceeds the average lifetime, which means most individuals will not leave their patch of origin during their lifetimes. Since the patches in this study are large and individual dispersal occurs on a small scale, this is reasonable. Third and last, we make the assumption that the migration rates are low enough not to cause equilibrium population densities in any patch

to exceed the region's carrying capacity. If this assumption is violated, and the carrying capacities are exceeded, the model equations would need to be adjusted to distribute the resulting negative logistic term (as a result of additional density-dependent deaths) proportionally between the susceptibles and infectives, since as discussed earlier the equations are written taking logistic terms to measure births only (generally supposed into the susceptible class). All of these assumptions can be viewed as upper bounds on the migration rates, but in practice these bounds do not interfere with the explorations at the heart of this investigation, since (as will be seen in Section 4) estimated migration rates are orders of magnitude smaller than the demographic rates.

We therefore derive the model given below and seen in Figure 1.

$$S'_{S3} = r_S \left(1 - \frac{N_{S3}}{K_{S3}}\right) N_{S3} - \beta_R \frac{I_{R3}}{N_{R3}} S_{S3} - (\mu_S + a_S) S_{S3} + \tilde{a}_S S_{S2}$$

$$I'_{S3} = \beta_R \frac{I_{R3}}{N_{R3}} S_{S3} - (\mu_S + b_S) I_{S3} + \tilde{b}_S I_{S2}$$

$$S'_{R3} = r_R \left(S_{R3} + (1 - p_R) I_{R3}\right) \left(1 - \frac{N_{R3}}{K_{R3}}\right) - \beta_S \frac{I_{S3}}{N_{R3}} S_{R3}$$
$$\qquad - (\mu_R + a_R) S_{R3} + \tilde{a}_R S_{R2}$$

$$I'_{R3} = p_R r_R I_{R3} \left(1 - \frac{N_{R3}}{K_{R3}}\right) + \beta_S \frac{I_{S3}}{N_{R3}} S_{R3} - (\mu_R + b_R) I_{R3} + \tilde{b}_R I_{R2}$$

$$S'_{S2} = r_S \left(1 - \frac{N_{S2}}{K_{S2}}\right) N_{S2} - \left(q_S \beta_R \frac{I_{R2}}{N_{R2}} + (1 - q_S) \beta_{WS} \frac{I_{W2}}{N_{W2}}\right) S_{S2}$$
$$\qquad - (\mu_S + \bar{a}_S) S_{S2} + \hat{a}_S S_{S3}$$

$$I'_{S2} = \left(q_S \beta_R \frac{I_{R2}}{N_{R2}} + (1 - q_S) \beta_{WS} \frac{I_{W2}}{N_{W2}}\right) S_{S2} - (\mu_S + \bar{b}_S) I_{S2} + \hat{b}_S I_{S3}$$

$$S'_{R2} = r_R \left(S_{R2} + (1 - p_R) I_{R2}\right) \left(1 - \frac{N_{R2}}{K_{R2}}\right) - \beta_{S2} \frac{I_{S2}}{N_{R2}} S_{R2}$$
$$\qquad - (\mu_R + \bar{a}_R) S_{R2} + \hat{a}_R S_{R3} \tag{1}$$

$$I'_{R2} = p_R r_R I_{R2} \left(1 - \frac{N_{R2}}{K_{R2}}\right) + \beta_{S2} \frac{I_{S2}}{N_{R2}} S_{R2} - (\mu_R + \bar{b}_R) I_{R2} + \hat{b}_R I_{R3}$$

$$S'_{G2} = r_G \left(1 - \frac{N_{G2}}{K_{G2}}\right) N_{G2} - \beta_{W2} \frac{I_{W2}}{N_{W2}} S_{G2} - (\mu_G + a_G) S_{G2} + \tilde{a}_G S_{G1}$$

$$I'_{G2} = \beta_{W2} \frac{I_{W2}}{N_{W2}} S_{G2} - (\mu_G + b_G) I_{G2} + \tilde{b}_G I_{G1}$$

$$S'_{W2} = r_W \left(S_{W2} + (1 - p_W) I_{W2}\right) \left(1 - \frac{N_{W2}}{K_{W2}}\right) - (\mu_W + a_W) S_{W2} + \tilde{a}_W S_{W1}$$
$$\qquad - \left((1 - q_W) \beta_G \frac{I_{G2}}{N_{W2}} + q_W \beta_{SW} \frac{I_{S2}}{N_{W2}}\right) S_{W2}$$

$$I'_{W2} = p_W r_W I_{W2} \left(1 - \frac{N_{W2}}{K_{W2}}\right) + \left((1 - q_W) \beta_G \frac{I_{G2}}{N_{W2}} + q_W \beta_{SW} \frac{I_{S2}}{N_{W2}}\right) S_{W2}$$
$$\qquad - (\mu_W + b_W) I_{W2} + \tilde{b}_W I_{W1}$$

$$S'_{G1} = r_G \left(1 - \frac{N_{G1}}{K_{G1}}\right) N_{G1} - \beta_W \frac{I_{W1}}{N_{W1}} S_{G1} - (\mu_G + \bar{a}_G) S_{G1} + \hat{a}_G S_{G2}$$

$$I'_{G1} = \beta_W \frac{I_{W1}}{N_{W1}} S_{G1} - (\mu_G + \bar{b}_G)I_{G1} + \hat{b}_G I_{G2}$$

$$S'_{W1} = r_W\left(S_{W1} + (1-p_W)I_{W1}\right)\left(1 - \frac{N_{W1}}{K_{W1}}\right) - \beta_G \frac{I_{G1}}{N_{W1}} S_{W1}$$
$$\qquad - (\mu_W + \bar{a}_W)S_{W1} + \hat{a}_W S_{W2}$$

$$I'_{W1} = p_W r_W I_{W1}\left(1 - \frac{N_{W1}}{K_{W1}}\right) + \beta_G \frac{I_{G1}}{N_{W1}} S_{W1} - (\mu_W + \bar{b}_W)I_{W1} + \hat{b}_W I_{W2}$$

3. **Analysis.** Little information is known about the migration of the vectors. Thus, we will explore several hypotheses. We will first consider that infected vectors are the only species to migrate. In a study done by Añez and East [2] in 1984 on the effect of parasites on the behavior of the vector *Rhodnius prolixus*, it was shown that that the parasite *Trypanosoma rangeli* hindered the vector's ability to draw blood, thus causing the bug to bite 25 more times than an uninfected vector. Thus, differential behavior of vectors infected with *T. cruzi* may affect the transmission of the parasite as well as vector mobility as mentioned in [29]. In this context, we will consider the possibility that infected vectors move in only one direction (towards more preferred climates) and the possibility that infected vectors move between patches at different rates for different directions. Furthermore, we consider that uninfected vectors also migrate, but at a rate proportional to that of infected vectors. We will not consider host migration to play a significant role. The hosts in the model are bound by habitat constraints, and thus by definition of the patches, we assume the hosts are not likely to cross patch boundaries.

In order to get a better understanding of the full model, several special cases will be considered. The main identifying characteristics of the model are vertical transmission, migration, and multiple hosts and vectors.

3.1. **One patch, one host, one vector, no vertical transmission.** We begin the analysis of (1) by studying the simple system with one host and one vector. By observing system (1), we see that when the migration terms $a_i = \bar{a}_i = b_j = \bar{b}_j = 0$, for $i = R, W$, $j = S, G$, the three patches decouple. In this scenario, patch 1 and patch 3 are identical in structure. Thus, analyzing patch 1 and 3 with migration terms set to 0 and $p_W = p_R = 0$, we are analyzing the simple one host-one vector system.

$$S'_h = r_h N_h \left(1 - \frac{N_h}{K_h}\right) - \beta_v \frac{I_v}{N_h} S_h - \mu_h S_h$$
$$I'_h = \beta_v \frac{I_v}{N_h} S_h - \mu_h I_h$$
$$S'_v = r_v N_v \left(1 - \frac{N_v}{K_v}\right) - \beta_h \frac{I_h}{N_h} S_v - \mu_v S_v \qquad (2)$$
$$I'_v = \beta_h \frac{I_h}{N_h} S_v - \mu_v I_v$$

Because the vector and host populations always approach an equilibrium, we can consider the limiting system in which N_h and N_v have reached their positive equilibria, N_h^* and N_v^*, where

$$N_h^* = K_h\left(1 - \frac{\mu_h}{r_h}\right), \quad N_v^* = K_v\left(1 - \frac{\mu_v}{r_v}\right).$$

As mentioned previously, for each species, we assume $r > \mu$, which guarantees that all disease-free extinction equilibria are unstable. This assumption will be carried out in this and all of the models hereafter. In system (2), we define $\tilde{\beta}_v = \beta_v \frac{N_v^*}{N_h^*}$. Results by Thieme [49, 50] guarantee that the behavior of the full system is asymptotic to the limiting system which is given by

$$
\begin{aligned}
I_h' &= \tilde{\beta}_v \frac{I_v}{N_v^*}(N_h^* - I_h) - \mu_h I_h \\
I_v' &= \beta_h \frac{I_h}{N_h^*}(N_v^* - I_v) - \mu_v I_v
\end{aligned}
\tag{3}
$$

This model has been well studied [46, 8] and we give results here. The basic reproductive number, calculated using the next-generation matrix [53], is given by

$$
R_0 = \sqrt{\frac{\beta_h \tilde{\beta}_v}{\mu_h \mu_v}},
$$

which represents the average number of secondary infections caused by an infected individual introduced into a susceptible population. Because of the vector-host dynamics, R_0 represents the geometric mean between the average number of secondary host infections caused by one vector, and the average number of vector infections caused by one host.

In the case when $R_0 < 1$, the disease will die out and the population will approach the disease free equilibrium. When $R_0 > 1$, the population will approach a unique endemic state,

$$
\frac{I_v^*}{N_v^*} = \frac{\beta_h \tilde{\beta}_v - \mu_h \mu_v}{\tilde{\beta}_v \beta_h + \tilde{\beta}_v \mu_v} = \frac{R_0^2 - 1}{R_0^2 + \frac{\tilde{\beta}_v}{\mu_h}},
$$

$$
\frac{I_h^*}{N_h^*} = \frac{\beta_h \tilde{\beta}_v - \mu_h \mu_v}{\tilde{\beta}_v \beta_h + \beta_h \mu_h} = \frac{R_0^2 - 1}{R_0^2 + \frac{\beta_h}{\mu_v}}.
$$

3.2. **Patch 2, no migration, no vertical transmission.** We will further analyze the decoupled system (1) by considering the equations representing patch 2 alone with no vertical transmission or migration. Thus, we analyze system (1) with $a_i = \bar{a}_i = 0$, for $i = R, W$, $b_j = \bar{b}_j = 0$, for $j = S, G$, and $p_R = p_W = 0$. The quantities N_{R2}, N_{S2}, N_{W2}, and N_{G2} are asymptotically constant to $N_{R2}^*, N_{S2}^*, N_{W2}^*$, and N_{G2}^*, respectively, where

$$
N_{S2}^* = K_{S2}\left(1 - \frac{\mu_S}{r_S}\right), \quad N_{R2}^* = K_{R2}\left(1 - \frac{\mu_R}{r_R}\right),
$$

$$
N_{G2}^* = K_{G2}\left(1 - \frac{\mu_G}{r_G}\right), \quad N_{W2}^* = K_{W2}\left(1 - \frac{\mu_W}{r_W}\right).
$$

Applying the results from Thieme [49, 50], we can study the limiting system

$$I'_{S2} = \left(q_S \beta_R \frac{I_{R2}}{N^*_{R2}} + (1 - q_S)\beta_{WS} \frac{I_{W2}}{N^*_{W2}} \right)(N^*_{S2} - I_{S2}) - \mu_S I_{S2},$$

$$I'_{R2} = \beta_{S2} \frac{I_{S2}}{N^*_{R2}}(N^*_{R2} - I_{R2}) - \mu_R I_{R2},$$

$$I'_{G2} = \beta_{W2} \frac{I_{W2}}{N^*_{W2}}(N^*_{G2} - I_{G2}) - \mu_G I_{G2}, \tag{4}$$

$$I'_{W2} = \left((1 - q_W)\beta_G \frac{I_{G2}}{N^*_{W2}} + q_W \beta_{SW} \frac{I_{S2}}{N^*_{W2}} \right)(N^*_{W2} - I_{W2}) - \mu_W I_{W2}.$$

System (4) exhibits the disease-free equilibrium $(I^*_{S2}, I^*_{R2}, I^*_{G2}, I^*_{W2}) = (0, 0, 0, 0)$. We find the basic reproductive number R_0 for the system using the next generation matrix method [53]. The work can be seen in Appendix A. We determine that

$$R_0 = \sqrt{\frac{1}{2}\left(P + \sqrt{P^2 - 4Q} \right)},$$

where

$$P = f_1 + f_2 + f_3, \quad Q = f_1 f_3, \quad f_1 = \frac{(1 - q_W)\beta_G \beta_{W2}}{\mu_G \mu_W} \frac{N^*_{G2}}{N^*_{W2}},$$

$$f_2 = \frac{q_W \beta_{SW} + (1 - q_S)\beta_{WS}}{\mu_S \mu_W} \frac{N^*_{S2}}{N^*_{W2}}, \quad f_3 = \frac{q_S \beta_R \beta_{S2}}{\mu_R \mu_S} \frac{N^*_{S2}}{N^*_{R2}}. \tag{5}$$

In the terms for R_0, we see that f_1 represents the *T. gerstaeckeri*-woodrat transmission cycle, f_2 represents the *T. sanguisuga*-woodrat cycle, and f_3 represents the *T. sanguisuga*-raccoon cycle. We further observe that

$$\max\{\sqrt{f_1}, \sqrt{f_2}, \sqrt{f_3}\} < R_0 < \sqrt{f_1 + f_2 + f_3}.$$

At this point, we wish to observe the importance of the overlap of the transmission cycles between *T. sanguisuga* and *T. gerstaeckeri*, and how this overlap affects the ability of the infection to be spread. If there is no overlap, i.e. no *T. sanguisuga*-woodrat cycle, then $f_2 = 0$, so then we may define $\bar{R}_0 = \sqrt{\max\{f_1, f_3\}} < R_0$. Since $\bar{R}_0$ is always less than R_0, we observe the effect of f_2 is to increase the value of R_0. It is possible that $f_1 < 1$ and $f_3 < 1$, yet $R_0 > 1$. Furthermore, it is also possible that $f_1 + f_3 < 1$, yet $R_0 > 1$.

By investigating the equilibrium conditions, it can be shown that either one or three endemic equilibrium values exist when $R_0 > 1$. The computations can be seen in Appendix A.

3.3. **Patches 1 and 2, 1 host 1 vector with vertical transmission and unidirectional migration of infected vectors.** In dealing with patches 1 and 2, there are several cases to be considered. We will first consider the scenario with one host and one vector, with vertical transmission, and unidirectional migration of infected vectors. In this case, $N_{R2} = N_{S2} = 0$, $q_W = q_S = 0$, and $a_W = \bar{a}_W = b_G = 0$. Because the woodrat population is asymptotically constant with $N^*_{W1} = K_{W1}\left(1 - \frac{\mu_W}{r_W}\right)$, $N^*_{W2} = K_{W2}\left(1 - \frac{\mu_W}{r_W}\right)$, we can apply Thieme's results [49, 50] and rewrite I'_{W1} and I'_{W2}, passing N_{W1} and N_{W2} to their limiting values,

N_{W1}^* and N_{W2}^*. The system therefore simplifies to

$$N_{G2}' = r_G N_{G2} \left(1 - \frac{N_{G2}}{K_{G2}} \right) - \mu_G N_{G2} + \tilde{b}_G I_{G1}$$

$$I_{G2}' = \beta_{W2} \frac{I_{W2}}{N_{W2}^*} (N_{G2} - I_{G2}) - \mu_G I_{G2} + \tilde{b}_G I_{G1}$$

$$I_{W2}' = p_W \mu_W I_{W2} + \beta_G \frac{I_{G2}}{N_{W2}^*} (N_{W2}^* - I_{W2}) - \mu_W I_{W2}$$

$$N_{G1}' = r_G N_{G1} \left(1 - \frac{N_{G1}}{K_{G1}} \right) - \mu_G N_{G1} - \bar{b}_G I_{G1} \qquad (6)$$

$$I_{G1}' = \beta_W \frac{I_{W1}}{N_{W1}^*} (N_{G1} - I_{G1}) - \mu_G I_{G1} - \bar{b}_G I_{G1}$$

$$I_{W1}' = p_W \mu_W I_{W1} + \beta_G \frac{I_{G1}}{N_{W1}^*} (N_{W1}^* - I_{W1}) - \mu_W I_{W1}$$

Cherif et al. [12] studied a similar model for *T. cruzi* vector transmission dynamics involving two strains (one being more virulent). In their model, a proportion of vectors infected with the more virulent strain migrate to a region in which the less virulent strain is native. However, their model did not include vertical transmission as system (6) does.

System (6) exhibits the disease-free equilibrium $(N_{G2}^*, 0, 0, N_{G1}^*, 0, 0)$, where

$$N_{G2}^* = K_{G2} \left(1 - \frac{\mu_G}{r_G} \right), \quad N_{G1}^* = K_{G1} \left(1 - \frac{\mu_G}{r_G} \right).$$

R_0 can be found via the next generation matrix. For system (6),

$$R_0 = \max \left\{ \frac{1}{2} \left(p_W + \sqrt{4 \frac{\beta_G \beta_W}{(\mu_G + \bar{b}_G) \mu_W} \frac{N_{G1}^*}{N_{W1}^*} + p_W^2} \right), \right.$$

$$\left. \frac{1}{2} \left(p_W + \sqrt{4 \frac{\beta_G \beta_{W2}}{\mu_G \mu_W} \frac{N_{G2}^*}{N_{W2}^*} + p_W^2} \right) \right\}.$$

If $\frac{N_{G1}^*}{N_{W1}^*} \leq \frac{N_{G2}^*}{N_{W2}^*}$ then the second term of R_0 is larger of the two because $\bar{b}_G > 0$. In this case $\max(p_W, \frac{\beta_G \beta_{W2}}{\mu_G \mu_W} \frac{N_{G2}^*}{N_{W2}^*}) < R_2 < p_W + \frac{\beta_G \beta_{W2}}{\mu_G \mu_W} \frac{N_{G2}^*}{N_{W2}^*}$.

To study possible endemic equilibria of system (6), we determine that

$$\bar{N}_{G2}^* = K_{G2} \left(1 - \frac{\mu_G - \tilde{b}_G x_{G1}^*}{r_G} \right), \quad \bar{N}_{G1}^* = K_{G1} \left(1 - \frac{\mu_G + \bar{b}_G x_{G1}^*}{r_G} \right)$$

After substituting these values into the equilibrium conditions for system (6) (seen in Appendix B), we determine existence of an endemic equilibrium when $R_0 > 1$. We further determine that precisely one endemic equilibria exist in patch 2 alone if and only if $R_1 < 1 < R_2$, and in both patches if $R_1 > 1$ (the patch 2 only endemic equilibrium is unstable in this case).

3.4. **Patches 1 and 2, 1 host and 1 vector with vertical transmission and unidirectional migration of uninfected and infected vectors.** We may also consider the case in which uninfected vectors move at a reduced rate proportional to that of infected vectors. As mentioned previously, if infected vectors exhibit differential behavior causing them to migrate more than uninfected vectors, we

would consider the effects of having uninfected vectors migrate as well, but at a reduced rate. We note that this scenario is as far as vertical transmission can be treated analytically regarding R_0. The vertical transmission terms in the model do not affect the complexity in computing endemic equilibria since μ is simply replaced with $(1-p)\mu$ in the infected host equations. Thus, in computing R_0, the remaining cases will be done without vertical transmission. We let $N_{R2} = N_{S2} = 0$, $q_W = q_S = 0$, $a_W = \bar{a}_W = 0$, and $b_G = \gamma \bar{b}_G$, where $0 < \gamma < 1$. Since N_{W1} and N_{W2} are asymptotically constant to $N_{W1}^* = K_{W1}\left(1 - \frac{\mu_W}{r_W}\right)$, $N_{W2}^* = K_{W2}\left(1 - \frac{\mu_W}{r_W}\right)$, we apply the results of Thieme to this system, passing N_{W1} and N_{W2} to their limiting values, N_{W1}^* and N_{W2}^*, and obtaining the following system,

$$S'_{G2} = r_G\left(1 - \frac{N_{G2}}{K_{G2}}\right)N_{G2} - \beta_{W2}\frac{I_{W2}}{N_{W2}}S_{G2} - \mu_G S_{G2} + \gamma \bar{b}_G S_{G1}$$

$$I'_{G2} = \beta_{W2}\frac{I_{W2}}{N_{W2}}S_{G2} - \mu_G I_{G2} + \tilde{b}_G I_{G1}$$

$$I'_{W2} = p_W\mu_W I_{W2} + \beta_G\frac{I_{G2}}{N_{W2}^*}(N_{W2}^* - I_{W2}) - \mu_W I_{W2}$$

$$S'_{G1} = r_G\left(1 - \frac{N_{G1}}{K_{G1}}\right)N_{G1} - \beta_W\frac{I_{W1}}{N_{W1}}S_{G1} - \mu_G S_{G1} - \gamma \bar{b}_G S_{G1} \qquad (7)$$

$$I'_{G1} = \beta_W\frac{I_{W1}}{N_{W1}}S_{G1} - \mu_G I_{G1} - \bar{b}_G I_{G1}$$

$$I'_{W1} = p_W\mu_W I_{W1} + \beta_G\frac{I_{G1}}{N_{W1}^*}(N_{W1}^* - I_{W1}^*) - \mu_W I_{W1}.$$

Here, we can determine the disease free equilibrium to be $(N_{G2}^*, 0, 0, N_{G1}^*, 0, 0)$, where

$$\frac{N_{G2}^*}{K_{G2}} = \sqrt{\left(1 - \frac{\mu_G}{r_G}\right)^2 + 4\frac{\gamma \bar{b}_G}{r_G}\frac{N_{G1}^*}{K_{G2}}\left(1 - \frac{\mu_G + \gamma \bar{b}_G}{r_G}\right)}, \quad \frac{N_{G1}^*}{K_{G1}} = \left(1 - \frac{\mu_G + \gamma \bar{b}_G}{r_G}\right).$$

Observing the terms of N_{G2}^*, we can see that the first term, $K_{G2}\left(1 - \frac{\mu_G}{r_G}\right)$, essentially represents the natural demographic renewal for the population of vectors in patch 2, while the second term represents the population being brought from vectors in patch 1.

R_0 for the system is $R_0 = \max\{R_1, R_2\}$ where

$$R_1 = \frac{1}{2}\left(p_W + \sqrt{4\frac{\beta_G\beta_W}{(\mu_G + \bar{b}_G)\mu_W}\frac{N_{G1}^*}{N_{W1}^*} + p_W^2}\right),$$

$$R_2 = \frac{1}{2}\left(p_W + \sqrt{4\frac{\beta_G\beta_{W2}}{\mu_G\mu_W}\frac{N_{G2}^*}{N_{W2}^*} + p_W^2}\right).$$

In general the form of R_0 for system (7) is the same as that of system (6), with a different disease free equilibrium for the vector population due to the unidirectional migration of all vectors. We see that the first term of R_0 represents the patch 1 dynamics, while the second term represents patch 2. Similar to the system in section 3.3, if $\frac{N_{G1}^*}{N_{W1}^*} \leq \frac{N_{G2}^*}{N_{W2}^*}$ then the second term of R_0 is larger.

Determining endemic equilibria for this system is intractable analytically. After a numerical investigation using the parameters estimated in section 4, we determine precisely one unique endemic equilibrium exists when $R_0 > 1$.

3.5. **Patch 1 and 2, 1 host 1 vector, no vertical transmission, bidirectional migration of infected vectors.** Another scenario we treat in patches 1 and 2 is one host, one vector and bidirectional migration of infected vectors. We have previously assumed that vectors may have a preferred direction so that our migration is unidirectional. However, we know that vectors will move in every direction (although one direction may be preferred over another); thus we consider bidirectional migration. In this system, $p_R = p_W = 0$, $q_W = q_S = 0$, $a_i = \bar{a}_i = 0$ for $i = R, W$. In this system, N_{W1} and N_{W2} are asymptotically constant to $N_{W1}^* = K_{W1}\left(1 - \frac{\mu_W}{r_W}\right)$, $N_{W2}^* = K_{W2}\left(1 - \frac{\mu_W}{r_W}\right)$. Applying the results by Thieme, we obtain the following system in which N_{W1} and N_{W2} have reached their limiting values.

The reduced system becomes

$$N'_{G2} = r_G N_{G2}\left(1 - \frac{N_{G2}}{K_{G2}}\right) - \mu_G N_{G2} - b_G I_{G2} + \tilde{b}_G I_{G1}$$

$$I'_{G2} = \beta_{W2}\frac{I_{W2}}{N_{W2}^*}(N_{G2} - I_{G2}) - (\mu_G + b_G)I_{G2} + \tilde{b}_G I_{G1}$$

$$I'_{W2} = \beta_G \frac{I_{G2}}{N_{W2}^*}(N_{W2}^* - I_{W2}) - \mu_W I_{W2}$$

$$N'_{G1} = r_G N_{G1}\left(1 - \frac{N_{G1}}{K_{G1}}\right) - \mu_G N_{G1} - \bar{b}_G I_{G1} + \hat{b}_G I_{G2} \tag{8}$$

$$I'_{G1} = \beta_W \frac{I_{W1}}{N_{W1}^*}(N_{G1} - I_{G1}) - (\mu_G + \bar{b}_G)I_{G1} + \hat{b}_G I_{G2}$$

$$I'_{W1} = \beta_G \frac{I_{G1}}{N_{W1}^*}(N_{W1}^* - I_{W1}) - \mu_W I_{W1}$$

We determine the disease-free equilibrium for this system (8) to be of similar form to that of (6).

R_0 for the system is given as follows:

$$R_0 = \sqrt{\frac{1}{2}\left((g_1 + g_2) + \sqrt{(g_1 + g_2)^2 - 4g_1 g_2 \epsilon}\right)}$$

where $\epsilon = \frac{\mu_G(\mu_G + b_G + \bar{b}_G)}{(\mu_G + b_G)(\mu_G + \bar{b}_G)} < 1$, $g_1 = \frac{\beta_G \beta_W}{\mu_G \mu_W}\frac{N_{G1}^*}{N_{W1}^*}\left(\frac{\mu_G + b_G}{\mu_G + b_G + \bar{b}_G}\right)$ and $g_2 = \frac{\beta_G \beta_{W2}}{\mu_G \mu_W}\frac{N_{G2}^*}{N_{W2}^*}$ $\left(\frac{\mu_G + \bar{b}_G}{\mu_G + b_G + \bar{b}_G}\right)$.

We observe that R_0 for system (8) is of similar form as the R_0 for system (4), with the exception of the migration terms. It is observed that $\max(\sqrt{g_1}, \sqrt{g_2}) < R_0 < \sqrt{g_1 + g_2}$. If either of the migration terms b_G or $\bar{b}_G$ is 0, then R_0 reduces to $\max(\sqrt{g_1}, \sqrt{g_2})$. We interpret g_1 as the basic reproductive number for patch 1 scaled by the proportion of infected vectors that stay in patch 1, and g_2 is the basic reproductive number for patch 2 scaled by the proportion of infected vectors staying in patch 2.

Determining existence of endemic equilibria is intractable analytically, but after a numerical investigation, we verify the hypothesis that in the case of bidirectional migration, only one endemic equilibria is possible if $R_0 > 1$.

3.6. **Patches 1 and 2, 2 hosts 2 vectors, no vertical transmission, unidirectional migration of infected vectors.** We end our exploration of two patches

by considering the case with 2 patches, 2 hosts, 2 vectors, and unidirectional migration of infected vectors. Then $p_R = p_W = 0$, $a_i = \bar{a}_i = 0$ for $i = R, W$ and $b_S = \bar{b}_S = b_G = 0$. In this scenario, the quantities N_{S2}, N_{R2}, N_{W2}, and N_{W1} are asymptotically constant to $N_{S2}^*, N_{R2}^*, N_{W2}^*$, and N_{W1}^*, respectively, where

$$\frac{N_{S2}^*}{K_{S2}} = \left(1 - \frac{\mu_S}{r_S}\right), \quad \frac{N_{R2}^*}{K_{R2}} = \left(1 - \frac{\mu_R}{r_R}\right), \quad \frac{N_{Wj}^*}{K_{Wj}} = \left(1 - \frac{\mu_W}{r_W}\right) \quad (j = 1, 2).$$

The model is

$$I_{S2}' = \left(q_S \beta_R \frac{I_{R2}}{N_{R2}^*} + (1 - q_S)\beta_{WS} \frac{I_{W2}}{N_{W2}^*}\right)(N_{S2}^* - I_{S2}) - \mu_S I_{S2}$$

$$I_{R2}' = \beta_{S2} \frac{I_{S2}}{N_{R2}^*}(N_{R2}^* - I_{R2}) - \mu_R I_{R2}$$

$$N_{G2}' = r_G N_{G2}\left(1 - \frac{N_{G2}}{K_{G2}}\right) - \mu_G N_{G2} + \tilde{b}_G I_{G1}$$

$$I_{G2}' = \beta_{W2} \frac{I_{W2}}{N_{W2}^*}(N_{G2}^* - I_{G2}) - \mu_G I_{G2} + \tilde{b}_G I_{G1}$$

$$I_{W2}' = \left((1 - q_W)\beta_G \frac{I_{G2}}{N_{W2}^*} + q_W \beta_{SW} \frac{I_{S2}}{N_{W2}^*}\right)(N_{W2}^* - I_{W2}) - \mu_W I_{W2} \tag{9}$$

$$N_{G1}' = r_G N_{G1}\left(1 - \frac{N_{G1}}{K_{G1}}\right) - \mu_G N_{G1} - \bar{b}_G I_{G1}$$

$$I_{G1}' = \beta_W \frac{I_{W1}}{N_{W1}^*}(N_{G1}^* - I_{G1}) - (\mu_G + \bar{b}_G)I_{G1}$$

$$I_{W1}' = \beta_G \frac{I_{G1}}{N_{W1}^*}(N_{W1}^* - I_{W1}) - \mu_W I_{W1}$$

For this scenario, the disease-free equilibrium is $(0, 0, N_{G2}^*, 0, 0, N_{G1}^*, 0, 0)$, where

$$N_{G2}^* = N_{G1}^* = K_G\left(1 - \frac{\mu_G}{r_G}\right).$$

After calculating R_0, the structure seen is similar to that of R_0 for system (4), and is given by

$$R_0 = \max\{R_1, R_2\},$$

where

$$R_1 = \sqrt{\frac{\beta_G}{(\mu_G + \bar{b}_G)} \frac{\beta_W}{\mu_W} \frac{N_{G1}^*}{N_{W1}^*}}, \quad R_2 = \sqrt{\frac{1}{2}\left(P + \sqrt{P^2 - 4Q}\right)}.$$

P and Q are the same expressions as those in (5).

We determine existence of endemic equilibria in patch 2 alone if and only if $R_1 < 1$ and $R_2 > 1$, and in both patches if and only if $R_1 > 1$. The computations can be seen in Appendix C.

3.7. Patch 1, 2, and 3, 2 hosts 2 vectors, no vertical transmission, unidirectional migration of infected vectors. We finally extend our discussion to all three patches. We now analyze the system represented by patch 1, 2, and 3, with 2 hosts, 2 vectors and unidirectional migration of infected vectors. Thus, we consider $p_i = 0$, $a_i = \bar{a}_i = 0$ for $i = R, W$ and $b_S = b_G = 0$. In this scenario, the host

populations, $N_{R3}, N_{R2}, N_{W2},$ and N_{W1} are asymptotically constant to the values

$$N_{R3}^* = K_{R3}\left(1 - \frac{\mu_R}{r_R}\right), \quad N_{R2}^* = K_{R2}\left(1 - \frac{\mu_R}{r_R}\right)$$

$$N_{W2}^* = K_{W2}\left(1 - \frac{\mu_W}{r_W}\right), \quad N_{W1}^* = K_{W1}\left(1 - \frac{\mu_W}{r_W}\right).$$

The reduced system becomes

$$N_{S3}' = r_S N_{S3}\left(1 - \frac{N_{S3}}{K_{S3}}\right) - \mu_S N_{S3} + \tilde{b}_S I_{S2}$$

$$I_{S3}' = \beta_R \frac{I_{R3}}{N_{R3}^*}(N_{S3} - I_{S3}) - \mu_S I_{S3} + \tilde{b}_S I_{S2}$$

$$I_{R3}' = \beta_S \frac{I_{S3}}{N_{R3}^*}(N_{R3}^* - I_{R3}) - \mu_R I_{R3}$$

$$N_{S2}' = r_S N_{S2}\left(1 - \frac{N_{S2}}{K_S}\right) - \mu_S N_{S2} - \bar{b}_S I_{S2}$$

$$I_{S2}' = \left(q_S\beta_R \frac{I_{R2}}{N_{R2}^*} + (1 - q_S)\beta_{WS} \frac{I_{W2}}{N_{W2}^*}\right)(N_{S2} - I_{S2}) - \mu_S I_{S2} - \bar{b}_S I_{S2}$$

$$I_{R2}' = \beta_{S2} \frac{I_{S2}}{N_{R2}^*}(N_{R2}^* - I_{R2}) - \mu_R I_{R2}$$

$$N_{G2}' = r_G N_{G2}\left(1 - \frac{N_{G2}}{K_{G2}}\right) - \mu_G N_{G2} + \tilde{b}_G I_{G1} \qquad (10)$$

$$I_{G2}' = \beta_{W2} \frac{I_{W2}}{N_{W2}^*}(N_{G2} - I_{G2}) - \mu_G I_{G2} + \tilde{b}_G I_{G1}$$

$$I_{W2}' = \left((1 - q_W)\beta_G \frac{I_{G2}}{N_{W2}^*} + q_W\beta_{SW} \frac{I_{S2}}{N_{W2}^*}\right)(N_{W2}^* - I_{W2}) - \mu_W I_{W2}$$

$$N_{G1}' = r_G N_{G1}\left(1 - \frac{N_{G1}}{K_{G1}}\right) - \mu_G N_{G1} - \bar{b}_G I_{G1}$$

$$I_{G1}' = \beta_W \frac{I_{W1}}{N_{W1}^*}(N_{G1} - I_{G1}) - \mu_G I_{G1} - \bar{b}_G I_{G1}$$

$$I_{W1}' = \beta_G \frac{I_{G1}}{N_{W1}^*}(N_{W1}^* - I_{W1}) - \mu_W I_{W1}$$

In analysis of system (10), we determine the disease free equilibrium to be $(N_{S3}^*, 0, 0, N_{S2}^*, 0, 0, N_{G2}^*, 0, 0, N_{G1}^*, 0, 0)$, where

$$N_{S3}^* = K_{S3}\left(1 - \frac{\mu_S}{r_S}\right), \quad N_{S2}^* = K_{S2}\left(1 - \frac{\mu_S}{r_S}\right),$$

$$N_{G2}^* = K_{G2}\left(1 - \frac{\mu_G}{r_G}\right), \quad N_{G1}^* = K_{G1}\left(1 - \frac{\mu_G}{r_G}\right).$$

We determine R_0 for this system to be $R_0 = \max\{R_1, R_2, R_3\}$, where

$$R_1 = \sqrt{\frac{\beta_G}{(\mu_G + \bar{b}_G)}\frac{\beta_W}{\mu_W}\frac{N_{G1}^*}{N_{W1}^*}}, \quad R_2 = \sqrt{\frac{1}{2}\left(P_2 + \sqrt{P_2^2 - 4Q_2}\right)}, \quad R_3 = \sqrt{\frac{\beta_R}{\mu_R}\frac{\beta_S}{\mu_S}\frac{N_{S3}^*}{N_{R3}^*}}$$

and $P_2 = h_1 + h_2 + h_3$, $Q_2 = h_1\, h_3$, with $h_1 = \dfrac{(1 - q_W)\beta_G}{\mu_G} \dfrac{\beta_{W2}}{\mu_W} \dfrac{N^*_{G2}}{N^*_{W2}}$,

$$h_2 = \frac{q_W \beta_{SW}}{(\mu_S + \overline{b}_S)} \frac{(1 - q_S)\beta_{WS}}{\mu_W} \frac{N^*_{S2}}{N^*_{W2}}, \quad h_3 = \frac{q_S \beta_R}{\mu_R} \frac{\beta_{S2}}{(\mu_S + \overline{b}_S)} \frac{N^*_{S2}}{N^*_{R2}}.$$

Based on the form of R_0, we would expect three different scenarios for existence of endemic equilibria. We expect existence of endemic equilibria in all three patches if and only if $R_1 > 1$, in patch 2 and 3 only if and only if $R_2 > 1$ and $R_1 < 1$, and in patch 3 only if and only if $R_3 > 1$, $R_1 < 1$, and $R_2 < 1$. Investigation of these scenarios can be seen in Appendix D, in which we are able to show existence of at least one endemic equilibrium for each of the scenarios mentioned above.

3.8. **Synthesis.** By analyzing many smaller, sub-models of the original system (1), we may make some generalizations regarding the behavior of the full model. We expect that the full system will exhibit classical threshold behavior regarding R_0, in which we expect a unique endemic equilibrium for $R_0 > 1$. As stated previously, the form of R_0 in a vector-borne disease is a geometric mean between infections caused by hosts and infections caused by vectors. If the system considers multiple hosts and vectors, the form of R_0 will include separate terms for each transmission cycle considered in the model. As described mathematically in section 3.3 and discussed in [29], we see vertical transmission has an "almost additive" effect on the basic reproductive number. Vertical transmission affects equilibria by effectively rescaling host mortality by a factor of $(1 - p)$, where p is the proportion of births to infected mothers in which vertical transmission occurs. In the case of unidirectional migration of infected vectors, we observe that R_0 consists of as many components as there are patches, and each component for R_0 contains parameters for only one patch. Also, as seen in section 3.7, multiple endemic equilibria are possible depending on the values of the patchwise reproductive numbers, R_1, R_2, R_3. We further note that by examination of (7), uninfected vectors migrating in one direction does not complicate the form of R_0. With bidirectional migration of infected vectors, we determine that the expression for R_0 involves contributions from all patches, rather than having a maximum of several components, which is to be expected since infection is moving in between patches. Based on this determination, we expect the full model to have one component for R_0, due to bidirectional migration; thus, it will not take on the form of $\max\{R_1, R_2, R_3\}$. In this case only one endemic equilibrium is possible; either there is no infection in any patch, or infection persists in all patches because all patches are connected by migration of infected vectors.

4. **Numerical results.**

4.1. **General demographic parameters.** We wish to investigate numerically the results of section 3, as well as investigate the behavior of the full model given by system (1). In order to do this, we will use biological information to estimate the parameters given in our model. Kribs-Zaleta [28] completed a thorough literature study to estimate demographic and *T. cruzi* infection related parameters regarding hosts and vectors in the United States. We will use the demographic quantities calculated in [28], given in Table 1.

We mention here that in our model, each host species has a preferred habitat. That is, the preferred habitat for the raccoons is patch 3; thus we would expect a higher population density of raccoons in patch 3 compared to patch 2. Similarly,

Species	μ	r
Raccoon	0.4/yr	0.90/yr
Woodrat	1/yr	1.8/yr
T. sanguisuga	0.271/yr	33/yr
T. gerstaeckeri	0.562/yr	100/yr

TABLE 1. Demographic parameters

Species	Population density	Carrying capacity
Woodrat	2300 rats/km^2	5200 rats/km^2
T. gerstaeckeri	31600 vectors/km^2	31900 vectors/km^2

TABLE 2. Patch 1 density estimates

the woodrat preferred habitat is prickly pear cactus which predominates in patch 1, with a lower density in patch 2 due to the varying landscapes. Here, we will treat the parameters that differ for each patch.

4.1.1. *Patch 1.* Kribs-Zaleta [28] obtains woodrat densities for Texas based on several sources [9, 44] which estimate woodrat population densities in counties in south and west Texas. These regions, especially the counties in west Texas, are similar to south Texas, dominated by shrub desert, including cactus and honey mesquite. He estimates the woodrat (equilibrium) population density in patch 1 to be 2300 woodrats/km^2. Because each population is governed by logistic growth with linear per-capita mortality, the populations approach an equilibrium population density, N^*, so that the carrying capacity can be back-calculated using $N^* = K \left(1 - \frac{\mu}{r}\right)$. Kribs-Zaleta estimates the total vector population density in patch 1 to be 31600 vectors/km^2. Since we are assuming that the only vector in our model in patch 1 is *T. gerstaeckeri*, we use this as the density estimate. Using these figures, we obtain patch 1 population density and carrying capacity estimates found in Table 2.

4.1.2. *Patch 2.* Estimates for southern plains woodrat density in patch 2 vary by geographical location and study. The woodrat density is affected by landscape, climate, and available materials for den construction. Raun [43] determined a positive correlation for population density of woodrats and density of cactus, although he concluded that cactus is not absolutely necessary to support woodrats. Cactus is the preferred material for den construction and food, but woodrats will use other materials to construct dens if cactus is unavailable [51]. In general, density of woodrat dens is closely associated with overhead cover.

In an 18 month study in Jim Wells Co., part of the Southern Texas Plains, Merkelz and Kerr [36] record a maximum density of 1.5 wr/ha (during spring 1998) using a 10 ha subplot of a 220 ha study site. Density was calculated by using the number of woodrats captured in the area during a single trapping season. Since they do not give any other density calculations, we use this data as part of our data collection. We note that they did not limit their density calculation to only areas with cactus growth so as to include open areas as part of the normal daily range of woodrats.

Conditt and Ribble [14] estimate a range of 1.6-5.8 wr/ha (average 3.7 wr/ha) in Bexar Co located in South Texas. The study was done on a 10 ha area of land

with 4 ha dominated by honey mesquite-brush and prickly pear cactus, while the remaining 6 ha dominated by riparian lowland forests. The density was calculated on the 4 ha site due to essentially no woodrats being found on the riparian forested area (cactus-free) of the study site. They mention that the low density may be due to lack of cactus in the region of study and lack of appropriate shelter sites. However, Raymond et al. [44] in 2003 calculate a much higher maximum density of 19.4 wr/ha (with an average of 15.1 wr/ha) in the same county (but a different study site). This study site had limited clumps of prickly pear, but was covered with thick brush and downed trees which served as nest sites. Thus, we see that cactus is not absolutely necessary to maintain a high population density, but rather an abundance of shelter sites.

Although we do not include Oklahoma in patch 2, due to the northern range of *T. gerstaeckeri*, we refer to a study in Harmon County, Oklahoma in the Mesquite Grass Plains region, in which the estimated woodrat density was 13 wr/ha [52]. This region is native to the southern plains woodrat, dominated by Mesquite and prickly-pear cactus. The population density estimate was determined by trapping at 104 of the known 1,129 woodrat houses in the 226 ha study plot, and the density of cactus was not taken into account for the woodrat population density estimate.

Raun [43] estimates a range of 14.8-31.4 woodrats/ha (average 23 wr/ha) in San Patricio Co, part of a transitional region between the Southern Texas Plains and Western Gulf Coastal Plain. Thus, the vegetation in this region is diverse, with the major plant communities being Mesquite-Mixedgrass, Chaparral-Mixedgrass, Live Oak-Chaparral, and Prickly Pear-Short grass, with riparian forests along the rivers [20, 7]. The study site, 9 acres, was reduced to 7.3 acres to estimate the density to eliminate areas that did not support cactus growth. A summary of these results can be found in Table 3.

Although there is a broad range of density estimates, we recall that patch 2 is a region with a diverse landscape, including mesquite, cactus, and savanna regions with areas of tree and prairie grassland. Since some estimates were computed in cactus-free regions, it is important to include each estimate in our computation of the average woodrat density. Thus, we include all 5 estimates in computing the average woodrat density in patch 2, obtaining an average population density of 11.3 wr/ha (1130 wr/km^2) in patch 2.

There are relatively few papers regarding raccoon distribution in patch 2. In a 3-year study by Gehrt and Fritzell [20], they estimate an average density of 7.3 raccoons/km^2 in San Patricio Co in southeast Texas. Since this region is not dominated by forest (as mentioned above), we would expect a lower raccoon density than that estimated by Kribs-Zaleta [28] for raccoon density in southeast USA (including patch 3). Using the equilibrium population densities, $N^* = K\left(1 - \frac{\mu}{r}\right)$, we calculate the carrying capacities for each species in patch 2, found in Table 4.

In patch 2, the *T. cruzi* transmission cycles overlap by the association of *T. sanguisuga* in association with both woodrats and raccoons, while *T. gerstaeckeri* feeds only on woodrats. The *T. sanguisuga* move between the woodrat and raccoon populations regularly enough that we will consider the *T. sanguisuga* a single population. We would like to estimate q_W, the proportion of vector-woodrat contacts in patch 2 that are with *T. sanguisuga*, while $1 - q_W$ is the proportion of vector-woodrat contacts that are *T. gerstaeckeri*. Also, since *T. sanguisuga* is associated with both hosts, we must estimate q_S, the proportion of *T. sanguisuga*-host contacts

Average density	Location	Ref
1.5 wr/ha	Jim Wells Co	[36]
3.7 wr/ha	Bexar Co	[14]
13 wr/ha	Southwestern OK	[52]
15.1 wr/ha	Bexar Co	[44]
23 wr/ha	San Patricio Co	[43]

TABLE 3. *Neotoma micropus* population density estimates

Species	Population density	Carrying capacity
Raccoon	7.3 racc/km^2	13.1 racc/km^2
Woodrat	1130 rats/km^2	2542.5 rats/km^2
All vectors	31600 vectors/km^2	31900 vectors/km^2

TABLE 4. Patch 2 density estimates

that are raccoons, with $1 - q_S$ the proportion of *T. sanguisuga*-host contacts made with woodrats.

Eads et al. [18] found 390 vectors from a total of 58 woodrat dens. Of the 390 vectors, 226 were *T. sanguisuga*, 133 were *T. gerstaeckeri*, and 31 were *T. neotomae*. We note here that the proportion of *T. neotomae* is negligible; thus we will normalize so that the proportions of *T. sanguisuga* and *T. gerstaeckeri* sum to 1. Thus, 63% of the vectors found in association with woodrats were *T. sanguisuga* and 37% were *T. gerstaeckeri*. Pippin [41] determined that for 85 woodrat dens, of 229 nymph and adult vectors, 58% were *T. sanguisuga*, while 42% were *T. gerstaeckeri*. If we pool the data, we determine 61% of the vector-woodrat contacts are with *T. sanguisuga*, and if we use the weighted average by number of dens excavated, the percentage is 60%. Thus, we estimate q_W to be 0.605.

To estimate q_S, we will define $q_S = \frac{N_{R2}^* \cdot V_R}{N_{R2}^* \cdot V_R + N_{W2}^* \cdot V_W}$, where N_{R2}^* is the patch 2 raccoon density and N_{W2}^* is the patch 2 woodrat density. V_R is the number of vectors per raccoon and V_W is the number of vectors per woodrat (scaled by the proportion that are *T. sanguisuga*). V_R can be estimated from the estimates given in [28]. We mention here that there are other hosts in patch 3, so not all *T. sanguisuga* can be found with raccoons. Ideally, we would calculate V_R directly to avoid biasing the estimates. Although raccoons are the preferred host of *T. sanguisuga*, the vector will feed on other hosts including opossums in patch 3. We will estimate the raccoon density equivalent of the opossum density. Based on literature reviews, we determine the population density of opossums to be 10.1/km^2 [28]. Thus, we determine the density of opossums is 0.505 times the raccoon density. We will divide the patch 3 *T. sanguisuga* population density, N_{S3}^*, estimated in [28] by the raccoon equivalent total host density. Using the estimates for N_{S3}^* and N_{R3}^* from [28], we determine $V_R = \frac{N_{S3}^*}{1.505 N_{R3}^*} = 1049.83$ *T. sanguisuga*/raccoon. Since both vector species are associated with woodrats, V_W is $q_W \frac{N_{G2}^* + N_{S2}^*}{N_{W2}^*}$. Kribs-Zaleta [28] estimates that the total *Triatoma* vector population in patch 2 is 31600 vectors/km^2. As estimated previously, $N_{W2}^* = 1130$ woodrats/km^2. These averages result in an estimate of V_W as 16.9 *T. sanguisuga*/woodrat. Based on this calculation, we arrive at an estimate of $q_S = 0.286$.

4.1.3. *Patch 3.* We use estimates from [28] for the raccoon and *T. sanguisuga* density estimates in patch 3, given in Table 5. We note here that the *T. sanguisuga* population density is based on a single study done by Burkholder et al. [10] regarding population density of *Triatoma* vectors, which estimates *Triatoma* density in relation to woodrat nests. Although *T. sanguisuga* in patch 3 are found with raccoons, we use the same estimate as the total vector population density in patches 1 and 2, due to lack of relevant information on vector population density in patch 3.

Species	Population density	Carrying capacity
Raccoon	20. racc/km^2	35.6 racc/km^2
T. sanguisuga	31600 vectors/km^2	31900 vectors/km^2

TABLE 5. Patch 3 density estimates

4.2. **Estimation of infection rate parameters.** The model here includes 2 modes of host infection: vertical transmission and direct transmission due to biting and to oral transmission via vector consumption. The vertical transmission parameters can be estimated directly via literature. Kribs-Zaleta [28] estimates the vertical transmission proportion to be 0.01. Then $p_W = 0.01$. We estimate $p_R = 0.1$ due to the adaptation of *T. cruzi* strain type IV to vertical transmission in raccoons. To estimate the direct infection rate parameters, we utilize the technique outlined in [28] to back-calculate the infection rate parameters, by solving for $\beta_R, \beta_S, \beta_{SW}, \beta_{WS}, \beta_G$, and β_W using the equilibrium conditions for model (1) under the assumption that observed prevalence indicates endemic equilibrium.

Since migration is small compared to the demographic processes, we will estimate the infection rate parameters by patch using model (1), assuming no migration. In order to estimate the infection rate parameters, we combine the observed prevalence levels and known demographic parameters in the equilibrium conditions to back-calculate the infection rate parameters, $\beta_R, \beta_S, \beta_{SW}, \beta_{WS}, \beta_{S2}, \beta_{W2}, \beta_G$, and β_W.

After a thorough literature search, Kribs-Zaleta calculates prevalence levels for each species in each patch. Prevalence levels for *T. gerstaeckeri* and the woodrat are given for Texas and levels for *T. sanguisuga* and raccoons are given for Texas and the southeast U.S. To translate these values to this model, we assume that the patch 1 and 2 prevalence levels for *T. gerstaeckeri* and southern plains woodrat are equivalent to the Texas estimates found in [29]. The patch 2 and 3 prevalence levels for *T. sanguisuga* and the raccoon are the same as the Texas and southeast estimates, respectively. A summary of these values is given in Table 6.

Species	Patch 1	Patch 2	Patch 3
Raccoon	-	0.240	0.387
T. sanguisuga	-	0.249	0.565
Woodrat	0.332	0.332	-
T. gerstaeckeri	0.454	0.454	-

TABLE 6. *T. cruzi* prevalence estimates from [28]

We note here that $x_{G1}^* = \frac{I_{G1}^*}{N_{G1}^*}$ is the prevalence value for *T. gerstaeckeri* in patch 1. We utilize a similar notation for the other 3 species in the model.
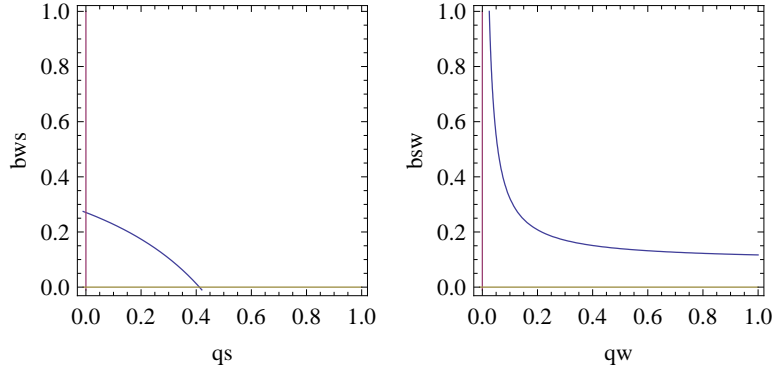
FIGURE 2. Correspondence of q_S and q_W with β_{WS}, with units 1/yr, and β_{SW}, with units infected hosts/vector/yr

Using the equilibrium conditions and substituting the population density estimates and prevalence values for patch 1,

$$\beta_W x^*_{W1}(1 - x^*_{G1}) - \mu_G x^*_{G1} = 0$$
$$p_W r_W x^*_{W1} \left(1 - \frac{N^*_{W1}}{K_{W1}}\right) + \beta_G x^*_{G1} \frac{N^*_{G1}}{N^*_{W1}}(1 - x^*_{W1}) - \mu_W x^*_{W1} = 0,$$

we obtain estimates for β_W and β_G, given in Table 7.

Substituting the patch 3 population density estimates and prevalence values into the patch 3 equilibrium conditions,

$$\beta_R x^*_{R3}(1 - x^*_{S3}) - \mu_S x^*_{S3} = 0$$
$$p_R r_R x^*_{R3} \left(1 - \frac{N^*_{R3}}{K_{R3}}\right) + \beta_S x^*_{S3} \frac{N^*_{S3}}{N^*_{R3}}(1 - x^*_{R3}) - \mu_R x^*_{R3} = 0,$$

we calculate β_R and β_S, given in Table 7.

Due to the crossover of infection cycles in patch 2, back-calculating the infection rate parameters is complex. After substituting the patch 2 equilibrium population densities and prevalence levels, there are 4 equilibrium conditions remaining:

$$(q_S \beta_R x^*_{R2} + (1 - q_S)\beta_{WS} x^*_{W2}) - \mu_S x^*_{S2} = 0$$
$$p_W r_W x^*_{W2} \left(1 - \frac{N^*_{W2}}{K_{W2}}\right) + \left((1 - q_W)\beta_G x^*_{G2} \frac{N^*_{G2}}{N^*_{W2}} + q_W \beta_{SW} x^*_{S2} \frac{N^*_{S2}}{N^*_{W2}}\right) \times$$
$$(1 - x^*_{W2}) - \mu_W x^*_{W2} N^*_{W2} = 0 \qquad (11)$$
$$p_R r_R x^*_{R2} \left(1 - \frac{N^*_{R2}}{K_{R2}}\right) + \beta_{S2} x^*_{S2}(1 - x^*_{R2}) \frac{N^*_{S2}}{N^*_{R2}} - \mu_R x^*_{R2} = 0$$
$$\beta_{W2} x^*_{W2}(1 - x^*_{G2}) - \mu_G x^*_{G2} = 0.$$

We note that there are six β values and four equations; thus the system is underdetermined. Consequently, we will assume that β_R and β_G have the same values in patch 2 as calculated in patches 3 and 1, respectively. After solving system (11), we determine values for β_{SW}, β_{WS}, β_{S2}, and β_{W2}, given in Table 7.

After an investigation of the effects of the proportions q_S and q_W on the β_{WS} and β_{SW} with all of the other parameters held fixed as determined above, we determine that any value of q_W greater than 0.3 will produce a value of β_{SW} in between 0.11/yr and 0.15/yr, which mitigates any inaccuracy in our estimate of $q_W = 0.605$. We also note that, mathematically, q_S needs to be smaller than 0.411 for β_{WS} to be positive, as seen in Figure 2.

Parameter	Value	Units
β_S	0.00025	
β_G	0.079	$\frac{\text{hosts}}{\text{vector}\cdot\text{yr}}$
β_{SW}	0.132	
β_{S2}	0.00017	
β_R	0.910	
β_W	1.408	1/yr
β_{WS}	0.116	
β_{W2}	1.408	

TABLE 7. Stercorarian infection rate parameters

Of the vector to host transmission terms, β_S and β_{S2} (vector to raccoon infection rate) are close in value, while β_G and β_{SW} (vector to woodrat infection rate) are close in value. But, we note here that there is a factor of 1000 by which woodrats are being infected more rapidly than raccoons are infected by $T.$ $sanguisuga$. We note this may be attributed partly to the fact that the population densities for woodrats are approximately 100 times as great as raccoon population densities. All of the host to vector transmission parameters are close in value, with the exception of β_{WS} (woodrat infecting $T.$ $sanguisuga$) which is an order of magnitude less than the raccoon to $T.$ $sanguisuga$ infection rates, which is to say that woodrats are infecting $T.$ $sanguisuga$ at a lower rate than raccoons infecting $T.$ $sanguisuga$.

4.3. Numerical solutions.

4.3.1. *Trends in migration rate effects.* To investigate the effects of migration numerically, we examine prevalence of $T.$ $cruzi$ as a function of vector migration. In order to get a clear picture, we first look at unidirectional migration of infected vectors. We then investigate unidirectional migration of all vectors as this is the upper bound of the possible unidirectional migration scenarios for vector migration. We then consider bidirectional migration of infected and all vectors. In each scenario, we consider the effects on $T.$ $cruzi$ prevalence as migration increases. To see the effects of the increase, we consider the effects of factor, k, multiplied by each migration rate. We calculate the prevalence for each patch as k increases from 0 to 10, where $k = 0$ represents the scenario with no migration and k increasing greater than 1 represents the migration rate increasing past the calculated rate from [15]. For each graph given, the host infected prevalence is represented by the lighter colored graph and the vector infected prevalence is represented by the darker colored graph.

In the case of northward migration of infected vectors (Figure 3), we observe a decrease of prevalence in patch 1 since this patch is losing infected vectors and not gaining any, and a slight increase of prevalence in patch 3 as the migration rate increases. The prevalence of $T.$ $sanguisuga$ in patch 2 is much lower than that in

patch 3, so although patch 3 is gaining infected vectors, the increase in prevalence at equilibrium is minimal.
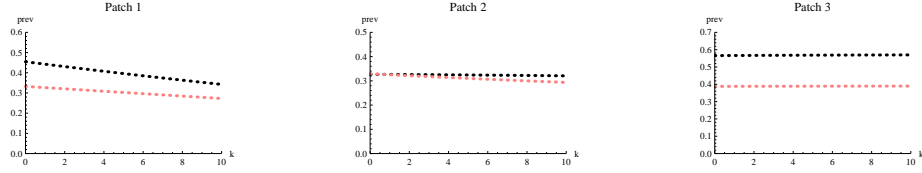

FIGURE 3. Equilibrium *T. cruzi* prevalence vs. vector migration rate multiplier for infected vectors migrating north only; dark curve represents vectors, light curve represents hosts
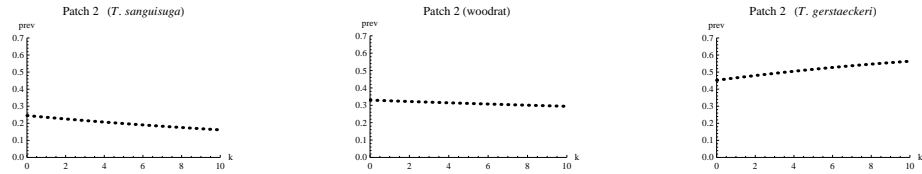

FIGURE 4. Equilibrium *T. cruzi* prevalence vs. vector migration rate multiplier for infected vectors moving north only (patch 2)

In this scenario, patch 2 is gaining infected vectors from patch 1(*T. gerstaeckeri*) and losing infected vectors to patch 3(*T. sanguisuga*). As seen in Figure 3, the patch 2 prevalence decreases for northward migration. To get a better understanding of why the prevalence decreases in patch 2, we look at the graphs of the prevalence for each vector species in patch 2, seen in Figure 4. It can be observed that the *T. sanguisuga* infected prevalence decreases by approximately 35% for high migration rates, while the *T. gerstaeckeri* prevalence increases by approximately 25%. Furthermore, we see a constant decrease in the woodrat prevalence (although *T. gerstackeri* prevalence increases). We note that in patch 2 N_{S2} is approximately 50% greater than N_{G2}. Thus, the export of infected *T. sanguisuga* from patch 2 dominates the import of infected *T. gerstaeckeri* from patch 1, causing an overall prevalence decrease in patch 2 in the case of northward migration of infected vectors.
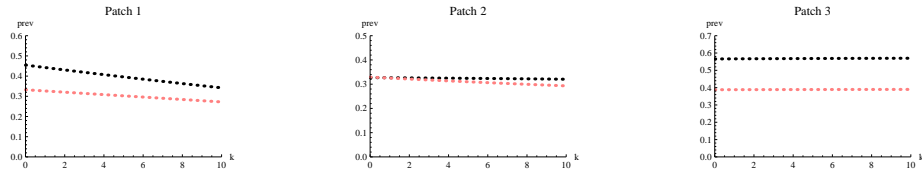

FIGURE 5. Equilibrium *T. cruzi* prevalence vs. vector migration rate multiplier for all vectors moving north only; dark curve represents vectors, light curve represents hosts

When we consider northward migration of all vectors, the change in prevalence is undetectable by viewing the graph. Patch 1 prevalence is still reduced since
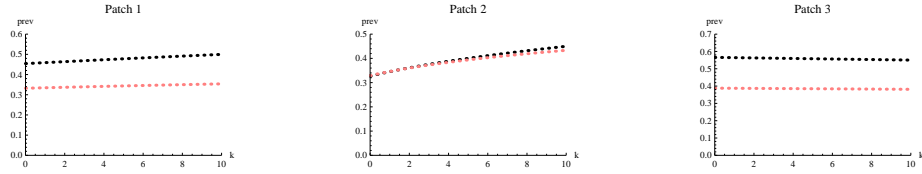
FIGURE 6. Equilibrium *T. cruzi* prevalence vs. vector migration rate multiplier for infected vectors moving south only; dark curve represents vectors, light curve represents hosts
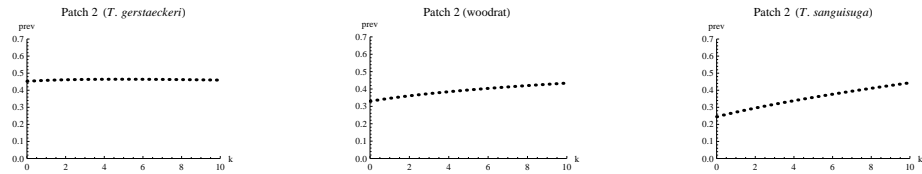

FIGURE 7. Equilibrium *T. cruzi* prevalence vs. vector migration rate multiplier for infected vectors moving south only (patch 2)

it is losing both infected and uninfected vectors, as seen in Figure 5. One might expect that the decrease should be less when all vectors are migrating, but after a numerical investigation of prevalence, we see that the decrease is slightly greater when all vectors are migrating. Also, we would expect the patch 3 prevalence to increase since this patch is gaining both infected and uninfected vectors from patch 2 with a lower prevalence; however the prevalence decreases slightly. If only infected vectors migrate northward, then R_1 decreases as $\bar{b}_G$ increases, causing prevalence in patch 1 to decrease. When all vectors are migrating northward, R_1 actually decreases more since the vector-host ratio is also decreasing, as the migration rate increases. Thus, the decrease in R_1 is amplified when all vectors are migrating northward.

As we observe southward migration of infected vectors, we again view the prevalence levels for each patch, in Figure 6. Patch 1 is gaining infected vectors from patch 2; thus we see an increase in prevalence. In patch 3, we see a slight decrease ($< 1\%$) in prevalence due to this patch losing infected vectors. In contrast to northward migration, we see a rise in prevalence for patch 2 in the case of southward migration. To understand why prevalence increases even though this patch is losing infected vectors to patch 1, we graph prevalence levels for each species in patch 2 as a function of migration, seen in Figure 7. We observe that prevalence in *T. sanguisuga* increases, as expected since this vector population is gaining infected vectors from patch 3. An interesting observation is that the prevalence in *T. gerstaeckeri* rises for small migration rates ($0 < k < 1$). Then, for higher migration rates, the prevalence for *T. gerstaeckeri* in patch 2 decreases. As observed in Figure 7, the woodrat *T. cruzi* prevalence increases in patch 2 for southward migration. Thus, for $0 < k < 1$, the sharp rise in prevalence in *T. sanguisuga* (11% increase) in patch 2 for small migration rates may be enough to increase the prevalence in *T. gerstaeckeri* through the woodrats.

In the case of southward migration of all vectors, the patch 3 prevalence decreases more than when only infected vectors are moving southward. This can be attributed
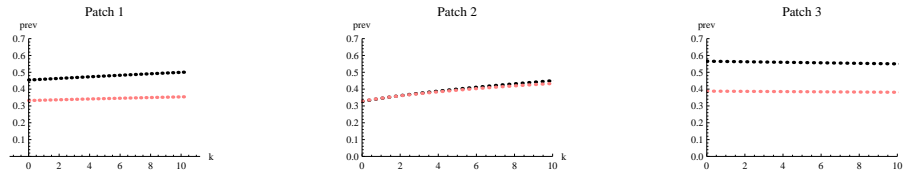
FIGURE 8. Equilibrium *T. cruzi* prevalence vs. vector migration rate multiplier for all vectors moving south only; dark curve represents vectors, light curve represents hosts
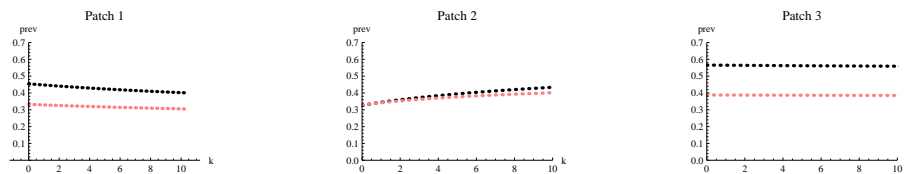

FIGURE 9. Equilibrium *T. cruzi* prevalence vs. vector migration rate multiplier for infected vectors bidirectional migration; dark curve represents vectors, light curve represents hosts
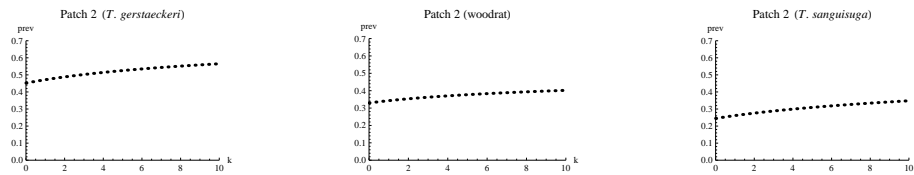

FIGURE 10. Equilibrium *T. cruzi* prevalence vs. vector migration rate multiplier for infected vectors bidirectional migration (patch 2)

to the decrease in vector-host ratio as the migration rate increases, thereby causing R_3 to decrease more than if only infected vectors are migrating. Patch 1 prevalence increases more than if only infected vectors are migrating southward, due to the slight increase in vector-host ratio. The patch 2 prevalence increases more than if only infected vectors are migrating southward, which is primarily due to the increase in vector-host ratio causing R_2 to increase more than if only infected vectors are migrating, as seen in Figure 8.

We also wish to investigate bidirectional migration of vectors. We first consider bidirectional migration of infected vectors only. As seen in Figure 9, prevalence decreases in patches 1 and 3, but increases in patch 2. To better understand why prevalence increases in patch 2, we observe the prevalence graphs for patch 2 only. We observe that both *T. sanguisuga* and *T. gerstaeckeri* prevalence increases in patch 2 (Figure 10).

The *T. sanguisuga* population in patch 2 is initially at a lower prevalence than patch 3, and since the *T. sanguisuga* population is gaining vectors from a patch with a higher prevalence, the prevalence increases for this species in patch 2 as seen in Figure 10. The *T. gerstaeckeri* prevalence also increases, although this population is
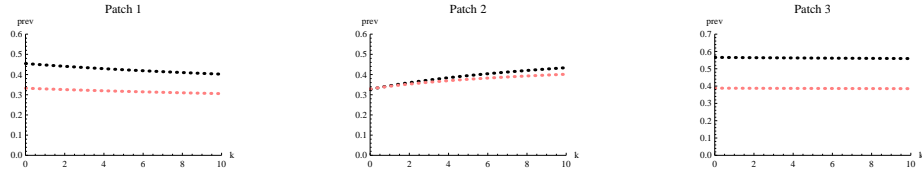
FIGURE 11. Equilibrium *T. cruzi* prevalence vs. vector migration rate multiplier for all vectors bidirectional migration; dark curve represents hosts, light curve represents vectors

gaining and losing vectors at the same prevalence. We can most likely attribute the increase in prevalence for *T. gerstaeckeri* in patch 2 due to the increase in woodrat prevalence (seen in Figure 10) through the *T. sanguisuga* prevalence increase.

In the case of bidirectional migration of all vectors, the behavior is similar. The patch 1 and 3 prevalence decreases slightly more than in the case of only infected vectors migration, due to the decrease of the vector-host ratio. A similar reason can be given for the patch 2 prevalence increasing more than if infected vectors are moving only.

4.3.2. *Calculation of the migration rate.* The framework established in [15] describes vector dispersal in terms of three properties: dispersal distance, preferred direction of dispersal, and degree of preference for a particular direction. Since we do not have clear data on a preference for a direction for *T. sanguisuga* and *T. gerstaeckeri*, we will consider the simplest case in which the vectors have no preference for direction of dispersal. Here we give the vector migration rates calculated in [15] assuming no preference for direction. We adjust these rates to take into account the area ratios and note that the rates are equal for all vectors (infected and susceptible) in each species.

$\bar{m}$	Species	rate
m_{12}	*T. gerstaeckeri*	0.00427
m_{21}	*T. gerstaeckeri*	0.00385
m_{23}	*T. sanguisuga*	0.00101
m_{32}	*T. sanguisuga*	0.000155

	Adjusted rate
$\tilde{b}_G = \tilde{a}_G$	0.00385
$\hat{b}_G = \hat{a}_G$	0.00427
$\tilde{b}_S = \tilde{a}_S$	0.000155
$\hat{b}_S = \hat{a}_S$	0.00101

TABLE 8. Migration rates for no preferred direction (units in 1/year)

We may also consider that vectors have a preference for direction of migration. Although we do not have clear evidence for the vectors in the model migrating with any clear trend in direction, we consider the possibility of vector migration in a particular direction. In a study on climate change related to Chagas disease distribution, Curto de Casas concludes that higher temperatures may extend the geographical range of the sylvatic vectors of *T. cruzi* [16]. Thus, we may consider vector migration with a northward preference for direction. We note here that when northward is described in section 4.3.1, it is referring to one-directional migration from patches 1 to 2 and 2 to 3, not the actual geographical direction north. In this section we are referring to the actual direction north and migration is bidirectional between patches.

Species	Equilibrium prevalence
Patch 3	
T. sanguisuga	0.56384
Raccoon	0.38513
Patch 2	
T. sanguisuga	0.24940
Raccoon	0.23628
T. gerstaeckeri	0.46649
Woodrat	0.33459
Patch 1	
T. gerstaeckeri	0.44686
Woodrat	0.32858

TABLE 9. Equilibrium prevalence levels for species based on migration (northward preference for direction)

The framework for deriving migration rates with a preference for direction is modeled using a sequence of nested ellipses, in which each ring represents a certain range of dispersal distances. We also assume that vectors have a degree of preference for a direction, which represents the eccentricity of each ellipse. Based on results from [15], we give results for *T. cruzi* prevalence assuming a northward preference of direction (with moderate degree of preference, $e = 0.5$) in Table 9. The decrease in prevalence in patch 1 and increase in prevalence for *T. gerstaeckeri* in patch 2 are consistent with what we expect assuming a northward preference for direction. We note that there is approximately a 1% decrease in prevalence for *T. sanguisuga* and raccoons in patch 2 if preferred direction is northward, when compared to migration with no preference for direction. There is a more than 3% increase in *T. gerstaeckeri* prevalence in patch 2 when compared to no migration. Although *T. gerstaeckeri* feeds only on woodrats, the increase in prevalence for *T. gerstaeckeri* is not enough to cause a higher increase in woodrat prevalence; thus we only observe only a slight (<1%) increase in prevalence for woodrats in patch 2 when the preferred direction of migration is northward.

5. **Conclusions.** Due to the complexity of system (1), several sub-models were analyzed in order to make conclusions regarding the behavior of the full model. The entire system appears to exhibit classical threshold behavior regarding R_0, and existence of a unique endemic equilibrium when $R_0 > 1$. In the case of one-directional migration of vectors, R_0 consists of as many components as there are patches with R_0 being the largest value of the patch-specific R_0 values, and multiple endemic equilibria are possible depending on the values of the patch-specific reproductive numbers values. If migration is bidirectional, R_0 will consist of only one component for containing parameters from all patches, and only one endemic equilibrium is possible; thus either the whole system reaches a disease-free state or infection persists in all patches. These results are similar to the multi-patch model results in [4], where it is shown that if patch a is at endemic equilibrium, then the disease is at endemic equilibrium in each patch accessible to patch a. Similar results are observed in the two-patch model in [3], where it is shown that if $R_0 < 1$, the disease does not persist in either population (patch), and if $R_0 > 1$, the disease persists in both populations.

In section 4, we obtained several different sets of results with respect to the effects of vector migration on the prevalence of *T. cruzi* in the geographical region from which we built our model. We examined the effects of one-directional migration, bidirectional migration (at symmetric rates), and bidirectional migration using rates derived from the framework in [15].

In the case of one-directional migration, the prevalence in the outer patches (patches 1 and 3) varies as expected (e.g. patch 1 prevalence decreases for northward migration only). However, the patch 2 dynamics are different for northward vs. southward migration. In the case of northward migration only, the patch 2 prevalence decreases while for southward migration, the prevalence increases. After closer observation of prevalence for each species in patch 2, it is determined that the *T. sanguisuga* migration has a greater effect on the patch 2 dynamics than the migration of *T. gerstaeckeri* primarily due to the fact that the difference in population density and prevalence in patches 2 and 3 among *T. sanguisuga* is greater than the difference in population density and prevalence in *T. gerstaeckeri* in patches 1 and 2. If vectors are migrating northward only, the export of *T. sanguisuga* dominates the import of *T. gerstaeckeri* thereby causing an overall decrease in patch 2 prevalence; we note that the *T. sanguisuga* population density in patch 2 is approximately 50% greater than the *T. gerstaeckeri* population density. For southward migration rates, the import of *T. sanguisuga* dominates the export of *T. gerstaeckeri* into patch 1. In fact, for lower migration rates, the prevalence for *T. gerstaeckeri* increases slightly due to the sharp increase in *T. sanguisuga* through the connection with the woodrat host. The connection between the vectors is the infection cycle with the woodrat host. Thus, the increase in prevalence for *T. gerstaeckeri* for lower southward migration rates is due to the increase in the prevalence for woodrats through the infection cycle with *T. sanguisuga*.

If migration is bidirectional, the patch 2 prevalence increases. After analysis of one-directional migration, the reason for the patch 2 prevalence increase is more apparent. We note here that the prevalence for *T. sanguisuga* is initially at a lower prevalence in patch 2 than in patch 3, so the *T. sanguisuga* in patch 2 is gaining vectors from a patch with a higher prevalence, thus the increase in *T. sanguisuga* prevalence. The prevalence for *T. gerstaeckeri* increases in patch 2 in the case of bidirectional migration due to the increase in woodrat prevalence (again through the infection cycle with *T. sanguisuga*). We note here that these trends are observed even if migration rates are considered symmetric (independent of patch size).

Because of the differences in patch sizes (especially the large size of patch 3 compared to patches 1 and 2), the vector density in each patch is affected differently by migration. For example, the change in patch 2 vector density will be greater than the change in patch 3 vector density for bidirectional migration. The patch 3 vector density is minimally affected by migration due to the large patch size.

Based upon these results we can conclude that infection dynamics in patch 2 are sensitive to migration, but primarily driven by the *T. sanguisuga* population. Since the same trends in prevalence change are observed for migration independent of patch size, we should investigate the distinctive transmission characteristics between host and vector. Thus, we consider differences in the *T. sanguisuga* and *T. gerstaeckeri* populations. One major difference in the vector populations is the high prevalence for *T. sanguisuga* in patch 3 compared to patch 2 and the prevalence for *T. gerstaeckeri*. If we assume no difference in prevalence levels for *T. sanguisuga* from patch 3 to 2, we can note that for southward migration, the prevalence in

patch 2 still increases for small migration rates, but at a much slower rate, while for northward migration, the prevalence decreases but at a much slower rate than if the prevalence in patch 3 is at its current estimated level. These results give a different picture for the patch 2 dynamics, which allow us to see a dampening effect of the *T. sanguisuga* migration if the prevalence levels for the *T. sanguisuga* populations in patches 2 and 3 are the same. Thus, we can attribute the majority of the patch 2 dynamics when migration is considered to the higher prevalence in *T. sanguisuga* in patch 3.

This aim of this study is to determine the effect of vector migration on *T. cruzi* transmission in the prominent sylvatic cycles ranging from northern Mexico to the southeastern United States. The primary effect of migration is to increase prevalence in the overlap patch where the prevalence is initially at a lower level than the outer (single-cycle) patches. The dominant force is the connection to the large raccoon-*T. sanguisuga* in the southeastern United States, which is affected little on such a large scale, but which can affect dynamics strongly in the overlap region with woodrats and *T. gerstaeckeri*.

As in every study, certain limitations must be noted. Due to the very recent awareness of the need to study *T. cruzi* in the United States, there have been very few studies on the demography of vectors native to the U.S., especially regarding vector population density. To date, there have been virtually no studies on the U.S. *Triatoma* vectors' dispersal or migration capabilities. Thus, with more studies, we may be able to more accurately describe the dispersal capabilities (especially regarding distance and frequency of vector flights). We acknowledge the need for more experimental or field studies with heavy consideration on the *Triatoma* vectors native to the United States, especially *T. gerstaeckeri* and *T. sanguisuga* which we consider to be the primary vectors in the southeast.

Because of the differing patch sizes, a natural question arises to consider effects of migration for higher spatial resolution where all patches are of uniform size. If the geographical region is broken into smaller, same-size patches, we wish to examine to what extent these results would change. Future work already in progress uses cellular automata to see how migration among smaller patches affects the spread of *T. cruzi* across a larger geographic region as well as determine a measure for speed of invasion. Although no data exist on large-scale vector migration patterns in this region, this work describes the geographical spread of *T. cruzi* under different migration scenarios.

REFERENCES

[1] Y. Benoist, P. Foulon and F. Labourie, Flots d'Anosov a distributions stable et instable differentiables, (French) [Anosov flows with stable and unstable differentiable distributions], *J. Amer. Math. Soc.*, **5** (1992), 33–74.

[2] N. Añez and J. S. East, Studies on *Trypanosoma rangeli* Tejera 1920 II. Its effect on feeding behaviour of triatomine bugs, *Acta tropica*, **41** (1984), 93–95.

[3] L. J. Allen, C. L. Wesley, R. D. Owen, D. G. Goodin, D. Koch, C. B. Jonsson, Y. Chu, J. M. Hutchinson and R. L. Paige, A habitat-based model for the spread of hantavirus between reservoir and spillover species, *Journal of Theoretical Biology*, **260** (2009), 510–522.

[4] J. Arino, J. R. Davis, D. Hartley, R. Jordan, J. M. Miller and P. van den Driessche, A multi-species epidemic model with spatial dynamics, *Mathematical Medicine and Biology*, **22** (2005), 129–142.

[5] C. B. Beard, G. Pye, F. J. Steurer, R. Rodriguiz, R. Campman, A. Townsend Peterson, J. Ramsey, R. A. Wirtz and L. E. Robinson, Chagas Disease in a domestic transmission cycle in southern Texas, USA, *Emerging Infectious Diseases*, **9** (2003), 103–105.

[6] C. Bern and S. P. Montgomery, An estimate of the burden of Chagas disease in the United States, *Clinical Infectious Diseases*, **49** (2009), 52–54.

[7] T. W. Box, Density of plains wood rat dens on four plant communities in south Texas, *Ecology*, **40** (1959), 715–716.

[8] F. Brauer, C. Castillo-Chavez and J. X. Velasco-Hernández, Recruitment effects in heterosexually transmitted disease models, *International Journal of Applied Science and Computation*, **3** (1996), 78–90.

[9] J. K. Braun and M. A. Mares, Neotoma micropus, *Mammalian Species*, **330** (1989), 1–9.

[10] J. E. Burkholder, T. C. Allison and V. P. Kelly, Trypanosoma cruzi (Chagas) (Protozoa: Kinetoplastida) in invertebrate, reservoir, and human hosts of the Lower Rio Grande Valley of Texas, *Journal of Parasitology*, **66** (1980), 305–311.

[11] Centers for Disease Control and Prevention (2012) *Chagas Disease*, Retrieved from http://www.cdc.gov/parasites/chagas

[12] A. Cherif, V. Garcia Horton, G. Melendez Rosario and W. Feliciano, *A Tale of Two Regions: A Mathematical Model for Chagas' Disease*, MTBI Technical Report MTBI 05-05M. Arizona State University 2008.

[13] C. G. Clark and O. J. Pung, Host specificity of ribosomal DNA variation in sylvatic *Trypanosoma cruzi* from North America, *Molecular and Biochemical Parisitology*, **66** (1994), 175–179.

[14] S. A. Conditt and D. O. Ribble, Social organization of *Neotoma micropus*, the southern plains woodrat, *Am. Midl. Nat.*, **137** (1996), 290–297.

[15] B. A. Crawford and C. M. Kribs-Zaleta, Vector migration and dispersal rate for sylvatic *T. cruzi* transmission, *Ecological Complexity*, **14** (2013), 145–156.

[16] S. I. Curto de Casas and R. U. Carcavallo, Climate change and vector-borne diseases distribution, *Social Science and Medicine*, **40** (1995), 1437–1440.

[17] P. L. Dorn, C. Monroy and A. Curtis, Triatoma dimidiata (Latreille, 1811): A review of its diversity across its geographic range and the relationship among populations, *Infection, Genetics and Evolution*, **7** (2007), 343–352.

[18] R. B. Eads, H. A. Trevino and E. G. Campos, Triatoma (Hemiptera:Reduviidae) Infected with *Trypanosoma Cruzi* in south Texas wood rat dens, *The Southwestern Naturalist*, **8** (1963), 38–42.

[19] E. K. Fritzell and K. J. Haroldson, Urocyon cinereoargenteus, *Mammalian Species*, **189** (1982), 1–8.

[20] S. D. Gehrt and E. K. Fritzell, Duration of familial bonds and dispersal patterns for raccoons in south Texas, *J. Mammalogy*, **79** (1998), 859–872.

[21] S. Gourbière, E. Dumonteil, J. E. Rabinovich, R. Minkoue and F. Menu, Demographic and dispersal constraints for domestic infestation by non-domiciled Chagas disease vectors in the Yucatan Peninsula, Mexico, *American Journal of Tropical Medicine and Hygiene*, **78** (2008), 133–139.

[22] J. M. Gurevitz, L. A. Ceballos, U. Kitron and R. E. Gürtler, Flight initiation of *Triatoma Infestans* (Hemiptera: Reduviidae) under natural climatic conditions, *Journal of Medical Entomology*, **43** (2006), 143–150.

[23] E. J. Hanford, F. B. Zhan, Y. Lu and A. Giordano, Chagas disease in Texas: Recognizing the significance and implications of evidence in the literature, *Social Science and Medicine*, **65** (2007), 60–79.

[24] M. Harry, F. Lema and C. A. Romaña, Chagas' disease challenge, *The Lancet*, **355** (2000), 236 pp.

[25] J. O. Ikenga and J. V. Richerson, Trypanosoma cruzi (Chagas) (Protozoa: Kinetoplastida: Trypanosomatidae) in invertebrate and vertebrate hosts from Brewster County in Trans-Pecos Texas, *Journal of Economic Entomology*, **77** (1984), 126–129.

[26] S. A. Kjos, K. F. Snowden and J. Olson, Biogeography and *Trypanosoma cruzi* infection prevalence of Chagas disease vectors in Texas, USA, *Vector-Borne and Zoonotic Diseases*, **9** (2009), 41–50

[27] C. Kribs Zaleta, Vector consumption and contact process saturation in sylvatic transmission of *T. cruzi*, *Mathematical Population Studies*, **13** (2006), 132–152.

[28] C. Kribs Zaleta, Estimating contact process saturation in sylvatic transmission of *Trypanosoma cruzi* in the U.S., *PLOS Neglected Tropical Diseases*, **4** (2010), 1–14.

[29] C. Kribs Zaleta, Alternative transmission modes for *Trypanosoma cruzi*, *Mathematical Bioscences and Engineering*, **7** (2010), 657–673.

[30] R. C. Lambert, K. N. Kolivras, L. M. Resler, C. C. Brewster and S. L. Paulson, The potential for emergence of Chagas disease in the United States, *Geospatial Health*, **2** (2008), 227–239.

[31] M. J. Lehane, P. K. McEwen, C. J. Whitaker and C. J. Schofield, The role of temperature and nutritional status in flight initiation by *Triatoma Infestans*, *Acta Tropica*, **52** (1992), 27–38.

[32] M. Lewis, J. Renclawowicz and P. van den Driessche, Traveling waves and spread rates for a West Nile virus model, *Bulletin of Mathematical Biology*, **68** (2006), 3–23.

[33] G. Macdonald, *The Epidemiology and Control of Malaria*, Oxford: Oxford University Press, 1957.

[34] N. A. Maidana and H. Mo Yang, Describing the geographic spread of dengue disease by traveling waves, *Mathematical Biosciences*, **215** (2008), 64–77.

[35] K. McBee and R. J. Baker, Dasypus novemcinctus, *Mammalian Species*, **162** (1982), 1–9.

[36] R. Merkelz and S. F. Kerr, Demographics, den use, movements, and absence of *Leishmania Mexicana* in southern plains woodrats *Neotoma micropus*, *The Southwestern Naturalist*, **47** (2002), 70–77.

[37] J. Milei, R. A. Guerri-Guttenberg, D. Rodolfo Grana and R. Storino, Prognostic impact of Chagas disease in the United States, *American Heart Journal*, **159** (2009), 22–29.

[38] E. Z. Moreno, I. M. Rivera, S. C. Moreno, M. E. Alarcón and A. Lugo-Yarbuh, Vertical transmission of *Trypanosoma cruzi* in Wistar rats during the acute phase of infection, *Investigación clínica (Maracaibo)*, **44** (2003).

[39] J. D.Murray, E. A. Stanely and D. L. Brown, On the spatial spread of rabies among foxes, *Precedings of the Royal Society of London*, **229** (1986), 111–1150.

[40] S. M. Pietzrak and O. J. Pung, Trypanosomiasis in raccoons from Georgia, *Journal of Wildlife Diseases*, **34** (1998), 132–136.

[41] W. F. Pippin, The biology and vector capability of *Triatoma Sanguisuga Texana Usinger* and *Triatoma Gerstaeckeri* (Stål)(Hemiptera: Triatominae), *Journal of Medical Entomology*, **7** (1970), 30–45.

[42] O. J. Pung, C. W. Banks, D. N. Jones and M. W. Krissinger, Trypanosoma cruzi in wild raccoons, opossums, and triatomine bugs in southeast Georgia, USA, *Journal of Parasitology*, **81** (1995), 583–587.

[43] G. G. Raun, A population of woodrats (*Neotoma micropus*) in southwest Texas, *Bull. Texas Mem. Mus.*, **11** (1966), 1–62.

[44] R. W. Raymond, C. P. McHugh, L. R. Witt and S. F. Kerr, Temporal and spatial distribution of *Leishmania mexicana* infections in a population of *Neotoma micropus*, *Mem. Inst. Oswaldo Cruz.*, **98** (2003), 171–180.

[45] D. M. Roellig, E. L. Brown, C. Barnabé, M. Tibayrenc, F. J. Steurer and M. J. Yabsley, Molecular typing of *Trypanosoma cruzi* isolates, United States, *Emerging Infectious Diseases*, **14** (2008), 1123–1125.

[46] R. Ross, *The Prevention of Malaria*, (2nd edition). London: Murray 1911.

[47] S. Sarkar, S. E. Strutz, D. M. Frank, C. L. Rivaldi, B. Sissel and V. Sánchez-Cordero, Chagas disease risk in Texas, *PLoS Neglected Tropical Diseases*, **4** (2010), 1–14.

[48] C. J. Schofield, M. J. Lehane, P. McEwen, S. S. Catala, and D. E. Gorla, Dispersive flight by *Triatoma Infestans* under natural climatic conditions in Argentina, *Medical and Veterinary Entomology*, **6** (1992), 51–56.

[49] H. R. Thieme, Convergence results and a Poincaré-Bendixson trichotomy for asymptotically autonomous differential equations, *Journal of Mathematical Biology*, **30** (1992), 755–763.

[50] H. R. Thieme, Asymptotically autonomous differential equations in the plane, *Rocky Mountain Journal of Mathematics*, **24** (1994), 351–380.

[51] K. M. Thies, M. L. Thies and W. Caire, House construction by the southern plains woodrat (*Neotoma micropus*) in southwestern Oklahoma, *The Southwestern Naturalist*, **41** (1996), 116–122.

[52] M. L. Thies and W. Caire, Nearest-neighbor analysis of the spatial distribution of houses *Neotoma micropus* in southwestern Oklahoma, *The Southwestern Naturalist*, **36** (1991), 233–262.

[53] P. van den Driessche and J. Watmough, Reproduction numbers and sub-threshold endemic equilibria for compartmental models of disease transmission, *Mathematical Biosciences*, **180** (2002), 29–48.

[54] J. X. Velasco-Hernàndez, An epidemiological model for the dynamics of Chagas' disease, *Biosystems*, **26** (1991), 127–134.

[55] M. E. Villagrán, C. Marin, A. Hurtado, M. Sánchez-Moreno and J. Antonio de Diego, Natural infection and distribution of Triatomines (Hemiptera: Reduviidae) in the state of Querétaro, Mexico, *The Royal Society of Tropical Medicine and Hygiene*, **102** (2008), 833–838.

[56] J. Wade-Smith and B. J. Verts, Mephitis mephitis, *Mammalian Species*, **173** (1982), 1–7.

[57] World Health Organization (2010) *Chagas Disease: American Trypanosomiasis*, Retrieved from http://www.who.int/mediacentre/factsheets/fs340/en

[58] M. Yabsley and G. Pittman Noblet, Biological and molecular characterization of a raccoon isolate of *Trypanosoma cruzi* from South Carolina, *Journal of Parasitology*, **88** (2002), 1273–1276.

[59] M. Yabsley, J. Barnes, A. Ellis, S. Kjos and C. Roxanne, Southern plains woodrats (*Neotoma micropus*) from southern Texas are important reservoirs of two genotypes of *Trypanosoma cruzi* and a host of a putative novel *Trypanosoma* species, *Vector-Borne and Zoonotic Diseases*, **13** (2012), 1–9.

[60] R. Zeledón, and J. E. Rabinovich, Chagas' Disease: An ecological appraisal with special emphasis on its insect vectors, *Annual Review of Entomology*, **26** (1981), 101–133.

[61] B. Zingales, S. G. Andrade, M. Briones, D. A. Campbell, E. Chiari, O. Fernandes, F. Guhl, E Lages-Silva, A. Macedo, C. R. Machado, M. A. Miles, A. J. Romanha, N. R. Sturm, M. Tibayrenc and A. G. Schijman, A new consensus for *Trypanosoma cruzi* intraspecific nomenclature: Second revision meeting recommends TcI to TcVI, *Mem. Inst. Oswaldo Cruz.*, **104** (2009), 1051–1054.

Appendix A. **Patch 2 with $p = 0$ and no migration.** We determine the reproductive number, R_0, for section 3.2, patch 2 with no vertical transmission or migration, using the next generation matrix method [53].

Based on the next generation matrix method, we rewrite system (4), $\frac{dX}{dt} = f(X)$ in terms of two vectors: $\frac{dX}{dt} = \mathcal{F}_0 - \mathcal{V}_0$. $\mathcal{F}_0$ represents the terms generating new infections, while $\mathcal{V}_0$ consists of the remaining terms. After computing the derivatives of $\mathcal{F}_0$ and $\mathcal{V}_0$, we obtain

$$F_0 = \begin{pmatrix} 0 & q_S \beta_R \frac{N_{S2}^*}{N_{R2}^*} & 0 & (1-q_S)\beta_{WS}\frac{N_{S2}^*}{N_{W2}^*} \\ \beta_{S2} & 0 & 0 & 0 \\ 0 & 0 & 0 & \beta_{W2}\frac{N_{G2}^*}{N_{W2}^*} \\ q_W \beta_{SW} & 0 & (1-q_W)\beta_G & 0 \end{pmatrix}$$

and

$$V_0 = \begin{pmatrix} \mu_S & 0 & 0 & 0 \\ 0 & \mu_R & 0 & 0 \\ 0 & 0 & \mu_G & 0 \\ 0 & 0 & 0 & \mu_W \end{pmatrix}.$$

The dominant eigenvalue of $F_0 V_0^{-1}$ is

$$R_0 = \sqrt{\frac{1}{2}\left(P + \sqrt{P^2 - 4Q}\right)},$$

where

$$P = f_1 + f_2 + f_3, \;\; Q = f_1 f_3, \;\; f_1 = \frac{(1-q_W)\beta_G \beta_{W2}}{\mu_G \mu_W}\frac{N_{G2}^*}{N_{W2}^*},$$

$$f_2 = \frac{q_W \beta_{SW}(1-q_S)\beta_{WS}}{\mu_S \mu_W}\frac{N_{S2}^*}{N_{W2}^*}, \;\; f_3 = \frac{q_S \beta_R \beta_{S2}}{\mu_R \mu_S}\frac{N_{S2}^*}{N_{R2}^*}. \tag{12}$$

It remains to be shown that $\sqrt{P^2 - 4Q}$ is real. Thus, we must show that $P^2 - 4Q > 0$, as follows:

$$
\begin{aligned}
P^2 - 4Q &= (f_1 + f_2 + f_3)^2 - 4f_1 f_3 \\
&= f_1^2 + f_2^2 + f_3^2 + 2f_1 f_2 + 2f_2 f_3 + 2f_1 f_3 - 4f_1 f_3 \\
&= f_1^2 - 2f_1 f_3 + f_3^2 + 2(f_1 f_2 + f_2 f_3) + f_2^2 \\
&= (f_1 - f_3)^2 + 2(f_1 f_2 + f_2 f_3) + f_2^2 > 0.
\end{aligned}
$$

To determine the existence of endemic equilibria, we determine the equilibrium conditions to be

$$
\begin{aligned}
(q_S \beta_R x_{R2}^* + (1 - q_S)\beta_{WS} x_{W2}^*)(1 - x_{S2}^*)N_{S2}^* - \mu_S x_{S2}^* N_{S2}^* &= 0, \\
\beta_{S2} x_{S2}^* N_{S2}^*(1 - x_{R2}^*) - \mu_R x_{R2}^* N_{R2}^* &= 0, \\
\beta_{W2} x_{W2}^*(1 - x_{G2}^*)N_{G2}^* - \mu_G x_{G2}^* N_{G2}^* &= 0, \\
((1 - q_W)\beta_G x_{G2}^* N_{G2}^* + q_W \beta_{SW} x_{S2}^* N_{S2}^*)(1 - x_{W2}^*) - \mu_W x_{W2}^* N_{W2}^* &= 0,
\end{aligned}
$$

(13)

where $x_{S2}^* = \frac{I_{S2}^*}{N_{S2}^*}$, $x_{R2}^* = \frac{I_{R2}^*}{N_{R2}^*}$, $x_{G2}^* = \frac{I_{G2}^*}{N_{G2}^*}$, and $x_{W2}^* = \frac{I_{W2}^*}{N_{W2}^*}$.

To simplify, we divide the 1st and 3rd equations by the nonzero values N_{S2}^* and N_{G2}^* respectively and make the substitutions, $\tilde{\beta}_G = (1 - q_W)\beta_G \frac{N_{G2}^*}{N_{W2}^*}$, $\tilde{\beta}_{SW} = q_W \beta_{SW} \frac{N_{S2}^*}{N_{W2}^*}$, and $\tilde{\beta}_{S2} = \beta_{S2} \frac{N_{S2}^*}{N_{R2}^*}$.

We solve the 2nd and 3rd equations for x_{R2}^* and x_{G2}^*:

$$
x_{R2}^* = \frac{\tilde{\beta}_{S2} x_{S2}^*}{\tilde{\beta}_{S2} x_{S2}^* + \mu_R} \quad \text{and} \quad x_{G2}^* = \frac{\beta_{W2} x_{W2}^*}{\beta_{W2} x_{W2}^* + \mu_G}
$$

We then solve the 1st equation in order to isolate x_{W2}^*. We obtain

$$
(\beta_R x_{R2}^* + (1 - q_S)\beta_{WS} x_{W2}^*)(1 - x_{S2}^*) - \mu_S x_{S2}^* = 0.
$$

Substituting the result for x_{R2}^* from above, we obtain

$$
\left[q_S \beta_R \left(\frac{\tilde{\beta}_{S2} x_{S2}^*}{\tilde{\beta}_{S2} x_{S2}^* + \mu_R} \right) + (1 - q_S)\beta_{WS} x_{W2}^* \right](1 - x_{S2}^*) - \mu_S x_{S2}^* = 0.
$$

Multiplying through on both sides by the denominator and combining like terms results in

$$
\begin{aligned}
&- (q_S \beta_R \tilde{\beta}_{S2} + \tilde{\beta}_{S2} \mu_S)(x_{S2}^*)^2 - (1 - q_S)\beta_{WS}\tilde{\beta}_{S2} x_{W2}^*(x_{S2}^*)^2 + (1 - q_S)\beta_{WS}\mu_R x_{W2}^* \\
&+ ((1 - q_S)\beta_{WS}\tilde{\beta}_{S2} - (1 - q_S)\beta_{WS}\mu_R)x_{W2}^* x_{S2}^* + ((1 - q_S)\beta_R \tilde{\beta}_{S2} - \mu_S \mu_R)x_{S2}^* = 0
\end{aligned}
$$

We then divide everything by μ_R and μ_S to obtain

$$
\begin{aligned}
&- \left(\frac{q_S \beta_R \tilde{\beta}_{S2}}{\mu_R \mu_S} + \frac{\tilde{\beta}_{S2}}{\mu_R} \right)(x_{S2}^*)^2 + \left(\frac{q_S \beta_R \tilde{\beta}_{S2}}{\mu_R \mu_S} - 1 \right) x_{S2}^* - \left(\frac{(1 - q_S)\beta_{WS}\tilde{\beta}_{S2}}{\mu_R \mu_S}(x_{S2}^2) \right. \\
&\left. - \left(\frac{(1 - q_S)\beta_{WS}\tilde{\beta}_{S2}}{\mu_R \mu_S} - \frac{(1 - q_S)\beta_{WS}}{\mu_S} \right) x_{S2}^* - \frac{(1 - q_S)\beta_{WS}}{\mu_S} \right) x_{W2}^* = 0.
\end{aligned}
$$

(14)

To simplify, we make the substitutions $A = \frac{q_S \beta_R}{\mu_S}$, $B = \frac{\tilde{\beta}_{S2}}{\mu_R}$, and $C = \frac{(1 - q_S)\beta_{WS}}{\mu_S}$ and solve for x_{W2}^* to obtain

$$
x_{W2}^* = \frac{x_{S2}^* \left[(A + 1)x_{S2}^* - A + \frac{1}{B} \right]}{C(1 - x_{S2}^*)\left(x_{S2}^* + \frac{1}{B} \right)}.
$$

(15)

We finally solve the 4th equation; substituting x^*_{G2}, we obtain

$$\left[\tilde{\beta}_G \left(\frac{\beta_{W2} x^*_{W2}}{\beta_{W2} x^*_{W2} + \mu_G} \right) + \tilde{\beta}_{SW} x^*_{S2} \right] (1 - x^*_{W2}) - \mu_W x^*_{W2} = 0.$$

Multiplying through by the denominator on both sides, we obtain

$$-(\tilde{\beta}_G \beta_{W2} + \beta_W \mu_W)(x^*_{W2})^2 - \tilde{\beta}_{SW} \beta_{W2} x^*_{S2}(x^*_{W2})^2 + (\tilde{\beta}_{SW} \beta_{W2} - \tilde{\beta}_{SW} \mu_G) x^*_{S2} x^*_{W2}$$
$$+ (\tilde{\beta}_G \beta_{W2} - \mu_G \mu_W) x^*_{W2} - \tilde{\beta}_{SW} \mu_G x^*_{S2} = 0,$$

and dividing all terms by μ_W and μ_G to get

$$-\left(\frac{\tilde{\beta}_G \beta_{W2}}{\mu_G \mu_W} + \frac{\beta_{W2}}{\mu_G} \right) (x^*_{W2})^2 + \left(\frac{\tilde{\beta}_G \beta_{W2}}{\mu_G \mu_W} - 1 \right) x^*_{W2}$$
$$-\left(\frac{\tilde{\beta}_{SW} \beta_{W2}}{\mu_G \mu_W} (x^*_{W2})^2 - \left(\frac{\tilde{\beta}_{SW} \beta_{W2}}{\mu_G \mu_W} - \frac{\tilde{\beta}_{SW}}{\mu_W} \right) x^*_{W2} - \frac{\tilde{\beta}_{SW}}{\mu_W} \right) x^*_{S2} = 0 \tag{16}$$

We make the substitutions $D = \frac{\tilde{\beta}_{SW}}{\mu_W}$, $E = \frac{\beta_W}{\mu_G}$, and $F = \frac{\tilde{\beta}_G}{\mu_W}$ and rewrite the previous equation as

$$(1 - x^*_{W2}) \left(x^*_{W2} + \frac{1}{E} \right) x^*_{S2} = \frac{1}{D} x^*_{W2} \left[(F+1) x^*_{W2} - F + \frac{1}{E} \right].$$

We can now determine a polynomial in x^*_{S2}, say $\phi(x^*_{S2})$. The resulting polynomial is of 4th degree, once the disease free equilibrium has been divided out, with constant term $\phi(0) = C(P - Q - 1)$, with P, Q as defined in (5), which is positive for $R_0 > 1$ by the following result

$$R_0^2 > 1$$
$$\frac{1}{2} \left[P + \sqrt{P^2 - 4Q} \right] > 1$$
$$\sqrt{P^2 - 4Q} > 2 - P$$
$$P^2 - 4Q > 4 - 4P + P^2$$
$$P - Q > 1$$

Therefore, since $\sqrt{P^2 - 4Q}$ is real, we have $R_0 > 1 \Leftrightarrow P - Q > 1$. Furthermore, it is observed that $\phi(1) < 0$ which implies that $\phi(x^*_{S2})$ crosses the x-axis 1 or 3 times between 0 and 1. By inspection of the form of x^*_{R2} and x^*_{G2}, we see that x^*_{R2} is in (0,1) if x^*_{S2} is in (0,1) and x^*_{G2} is in (0,1) if x^*_{W2} is. Alternatively, we can use the equations (14) and (16) to obtain a polynomial in x^*_{W2} and apply the same technique. Thus, there are either 1 or 3 endemic equilibria for this system when $R_0 > 1$. Thus, if $(x^*_{S2}, x^*_{W2}) \in [0,1] \times [0,1]$, then the remaining values, x^*_{R2} and x^*_{G2} are also in $[0,1]$.

Appendix B. **Patches 1 and 2, 1 host 1 vector, with VT, unidirectional migration of infected vectors.** To determine the basic reproductive number for section 3.3, we apply the next generation matrix method [53] to (6). We determine

the relevant matrices to be

$$F_1 = \begin{pmatrix} 0 & 0 & \beta_{W2}\frac{N_{G2}^*}{N_{W2}^*} & 0 \\ 0 & 0 & 0 & \beta_W\frac{N_{G1}^*}{N_{W1}^*} \\ \beta_G & 0 & p_W r_W\left(1 - \frac{N_{W2}^*}{K_W}\right) & 0 \\ 0 & \beta_G & 0 & p_W r_W\left(1 - \frac{N_{W1}^*}{K_W}\right) \end{pmatrix}$$

and

$$V_1 = \begin{pmatrix} \mu_G & -\tilde{b}_G & 0 & 0 \\ 0 & \mu_G + \bar{b}_G & 0 & 0 \\ 0 & 0 & \mu_W & 0 \\ 0 & 0 & 0 & \mu_W \end{pmatrix}.$$

After computing $F_1 V_1^{-1}$, we obtain the dominant eigenvalue as

$$R_0 = \max\left\{ \frac{1}{2}\left(p_W + \sqrt{4\frac{\beta_G\beta_W}{(\mu_G + \bar{b}_G)\mu_W}\frac{N_{G1}^*}{N_{W1}^*} + p_W^2}\right), \right.$$
$$\left. \frac{1}{2}\left(p_W + \sqrt{4\frac{\beta_G\beta_{W2}}{\mu_G\mu_W}\frac{N_{G2}^*}{N_{W2}^*} + p_W^2}\right)\right\}.$$

To study the existence of endemic equilibria, we first determine

$$\bar{N}_{G2}^* = K_G\left(1 - \frac{\mu_G - \tilde{b}_G x_{G1}^*}{r_G}\right), \quad \bar{N}_{G1}^* = K_G\left(1 - \frac{\mu_G + \bar{b}_G x_{G1}^*}{r_G}.\right)$$

The remaining equilibrium conditions are given by

$$\begin{aligned} \beta_{W2}x_{W2}^*(1 - x_{G2}^*)\bar{N}_{G2}^* - \mu_G x_{G2}^*\bar{N}_{G2}^* + \tilde{b}_G x_{G1}^*\bar{N}_{G1}^* &= 0 \\ \beta_G x_{G2}^*\bar{N}_{G2}^*(1 - x_{W2}^*) - \mu_W x_{W2}^* N_{W2}^*(1 - p_W) &= 0 \\ \beta_W x_{W1}^*(1 - x_{G1}^*)\bar{N}_{G1}^* - \mu_G x_{G1}^*\bar{N}_{G1}^* - \bar{b}_G x_{G1}^*\bar{N}_{G1}^* &= 0 \\ \beta_G x_{G1}^*\bar{N}_{G1}^*(1 - x_{W1}^*) - \mu_W x_{W1}^* N_{W1}^*(1 - p_W) &= 0 \end{aligned} \tag{17}$$

As $\bar{N}_{G1}^* = K_G\left(1 - \frac{\mu_G + \bar{b}_G x_{G1}^*}{r_G}\right) \neq 0$ since $r_G > \mu_G + \bar{b}_G$, we can divide both sides of the 3rd equation by $\bar{N}_{G1}^*$ to obtain

$$x_{G1}^* = \frac{\beta_W x_{W1}^*}{\beta_W x_{W1}^* + \mu_G + \bar{b}_G}.$$

It can be seen that if $0 \leq x_{W1}^* < 1$, then $0 \leq x_{G1}^* < 1$. To show $0 < x_{W1}^* < 1$, we substitute this expression for x_{G1}^* into the 4th equation in the equilibrium conditions and expand to obtain a cubic polynomial in x_{W1}^*. We can factor out the disease free equilibrium (in patch 1), in which $x_{W1}^* = 0$ leads us to the simple one host one vector patch 2 only endemic equilibrium. Thus, if $R_1 < 1 < R_2$, we have existence of precisely one endemic equilibrium. Otherwise, for $x_{W1}^* > 0$, our resulting quadratic polynomial is $\zeta(x_{W1}^*) = a_2 x_{W1}^{*2} + a_1 x_{W1}^* + a_0 = 0$ with

$$a_0 = r_G\mu_W N_{W1}^*(\bar{b}_G + \mu_G)^2\left(\frac{\beta_G\beta_W N_{G1}^*}{(\bar{b}_G + \mu_G)\mu_W N_{W1}^*} + p_W - 1\right),$$

$a_1 = -\beta_W$
$[\beta_G K_G((\mu_G + \bar{b}_G)(r_G - \mu_G) - \beta_W(r_G - (\mu_G + \bar{b}_G))) + 2(\mu_G + \bar{b}_G)r_G\mu_W N_{W1}^*(1 - p_W)],$
$$a_2 = -\beta_W^2[\beta_G K_G(r_G - (\mu_G + \bar{b}_G)) + r_G\mu_W N_{W1}^*(p_W - 1)]$$

We first observe that the constant term, $\zeta(0) = a_0$ is positive if and only if $R_1 > 1$ by the result below:

$$R_1 > 1$$

$$\frac{1}{2}\left(p_W + \sqrt{4\frac{\beta_G\beta_W N^*_{G1}}{(\mu_G + \bar{b}_G)\mu_W N^*_{W1}} + p^2_W}\right) > 1$$

$$\left(p_W + \sqrt{4\frac{\beta_G\beta_W N^*_{G1}}{(\mu_G + \bar{b}_G)\mu_W N^*_{W1}} + p^2_W}\right) > 2$$

$$\sqrt{4\frac{\beta_G\beta_W N^*_{G1}}{(\mu_G + \bar{b}_G)\mu_W N^*_{W1}} + p^2_W} > 2 - p_W$$

$$4p_W + 4\frac{\beta_G\beta_W N^*_{G1}}{(\mu_G + \bar{b}_G)\mu_W N^*_{W1}} - 4 > 0$$

$$p_W + \frac{\beta_G\beta_W N^*_{G1}}{(\mu_G + \bar{b}_G)\mu_W N^*_{W1}} - 1 > 0$$

Furthermore $\zeta(1) < 0$. Thus, we can conclude that $\zeta(x^*_{W1})$ crosses the x-axis precisely once between 0 and 1.

In order to show that $0 \leq x^*_{G2} < 1$ and $0 \leq x^*_{W2} < 1$, we solve the first equilibrium condition for x^*_{G2} in terms of x^*_{W2} and x^*_{G1},

$$x^*_{G2} = \frac{\beta_{W2}x^*_{W2}\bar{N}^*_{G2} + \tilde{b}_G x^*_{G1} N^*_{G1}}{\beta_{W2}x^*_{W2}\bar{N}^*_{G2} + \mu_G \bar{N}^*_{G2}}$$

$$= \frac{\beta_{W2}x^*_{W2} + \tilde{b}_G x^*_{G1}\frac{\bar{N}^*_{G1}}{\bar{N}^*_{G2}}}{\beta_{W2}x^*_{W2} + \mu_G}$$

We note that if x^*_{W2} is in $(0, 1)$, $\frac{\bar{N}^*_{G1}}{\bar{N}^*_{G2}} < 1$ and $\mu_G > \bar{b}_G$, then $0 \leq x^*_{G2} < 1$. To show $0 \leq x^*_{W2} < 1$, we substitute the expression for x^*_{G2} into the 2nd equilibrium condition from (17):

$$\eta(x^*_{W2}) = -(\beta_G\beta_{W2}\bar{N}^*_{G2} + \beta_{W2}\mu_W(1 - p_W)N^*_{W2})(x^*_{W2})^2$$
$$+ [\beta_G\beta_{W2}\bar{N}^*_{G2} - \mu_G\mu_W(1 - p_W)N^*_{W2} - \beta_G\tilde{b}_G x^*_{G1}\bar{N}^*_{G1}]x^*_{W2} + \beta_G\tilde{b}_G x^*_{G1}\bar{N}^*_{G1} = 0.$$

Since we have shown $0 \leq x^*_{G1} < 1$ and $\bar{N}^*_{G2}, \bar{N}^*_{G1}$, and N^*_{W2} are all nonzero, positive constants, it is clear that $\eta(0) = \beta_G\tilde{b}_G x^*_{G1}\bar{N}^*_{G1} > 0$ and $\eta(1) = -(1 - p_W)\mu_W N^*_{W2}(\beta_{W2} + \mu_G) < 0$. Thus, $\eta(x^*_{W2})$ crosses the x-axis precisely once between 0 and 1. Thus, $0 \leq x^*_{W2} < 1$ which implies that $0 \leq x^*_{G2} < 1$, so that there exists precisely one endemic equilibrium value for system (6) when $R_1 > 1$.

If $R_1 < 1$, we observe that the constant term, $\zeta(0) = a_0$, is negative. Furthermore, $\zeta(1)$ is also negative. Thus, ζ has either 0 or 2 roots between 0 and 1. After a numerical investigation using the parameters estimated in section 4, we determine that both roots of ζ are always negative for $R_1 < 1$, thus no roots are in (0,1).

Appendix C. **Patches 1 and 2, 2 hosts 2 vectors, no VT, unidirectional migration of infected vectors.** We wish to determine existence of endemic equilibria for section 3.6, system (9). We first determine that

$$N_{G2}^* = K_{G2}\left(1 - \frac{\mu_G - \tilde{b}_G x_{G1}^*}{r_G}\right), \quad N_{G1}^* = K_{G1}\left(1 - \frac{\mu_G + \bar{b}_G x_{G1}^*}{r_G}\right).$$

We then wish to solve the remaining equilibrium conditions given by

$$\begin{aligned}
(q_S\beta_R x_{R2}^* + (1-q_S)\beta_{WS}x_{W2}^*)(1-x_{S2}^*)N_{S2}^* - \mu_S x_{S2}^* N_{S2}^* &= 0 \\
\beta_S x_{S2}^* N_{S2}^*(1-x_{R2}^*) - \mu_R x_{R2}^* N_{R2}^* &= 0 \\
\beta_{W2}x_{W2}^*(1-x_{G2}^*)N_{G2}^* - \mu_G x_{G2}^* N_{G2}^* + \tilde{b}_G x_{G1}^* N_{G1}^* &= 0 \\
((1-q_W)\beta_G x_{G2}^* N_{G2}^* + \tilde{\beta}_{SW}x_{S2}^* N_{S2}^*)(1-x_{W2}^*) - \mu_W x_{W2}^* N_{W2}^* &= 0 \\
\beta_W x_{W1}^*(1-x_{G1}^*)N_{G1}^* - (\mu_G + \bar{b}_G)x_{G1}^* N_{G1}^* &= 0 \\
\beta_G x_{G1}^* N_{G1}^*(1-x_{W1}^*) - \mu_W x_{W1}^* N_{W1}^* &= 0
\end{aligned} \quad (18)$$

To simplify, we make the substitution $\tilde{\beta}_{SW} = q_W\beta_{SW}\frac{N_{S2}^*}{N_{W2}^*}$ and $\tilde{\beta}_{S2} = \beta_{S2}\frac{N_{S2}^*}{N_{R2}^*}$.

$$\begin{aligned}
(q_S\beta_R x_{R2}^* + (1-q_S)\beta_{WS}x_{W2}^*)(1-x_{S2}^*) - \mu_S x_{S2}^* &= 0 \\
\tilde{\beta}_{S2}x_{S2}^*(1-x_{R2}^*) - \mu_R x_{R2}^* &= 0 \\
\beta_{W2}x_{W2}^*(1-x_{G2}^*) - \mu_G x_{G2}^* + \tilde{b}_G x_{G1}^*\frac{N_{G1}^*}{N_{G2}^*} &= 0 \\
((1-q_W)\beta_G x_{G2}^*\frac{N_{G2}^*}{N_{W2}^*} + \tilde{\beta}_{SW}x_{S2}^*)(1-x_{W2}^*) - \mu_W x_{W2}^* &= 0 \\
\beta_W x_{W1}^*(1-x_{G1}^*)N_{G1}^* - (\mu_G + \bar{b}_G)x_{G1}^* N_{G1}^* &= 0 \\
\beta_G x_{G1}^* N_{G1}^*(1-x_{W1}^*) - \mu_W x_{W1}^* N_{W1}^* &= 0
\end{aligned} \quad (19)$$

In system (19), the last 2 equations decouple from the system, so we may study those equations separately. By inspection, we see that the last two equations are identical to the last two equations of (17) with $p_W = 0$. From analysis of (17) we see that either $x_{G1}^* = x_{W1}^* = 0$ or $R_1 > 1$. In this patch alone, one unique endemic equilibrium exists if and only if $R_1 > 1$ (as shown in Appendix B for system (17)).

If $x_{G1}^* = x_{W1}^* = 0$, we determine the remaining equilibrium conditions

$$\begin{aligned}
(q_S\beta_R x_{R2}^* + (1-q_S)\beta_{WS}x_{W2}^*)(1-x_{S2}^*) - \mu_S x_{S2}^* &= 0 \\
\tilde{\beta}_{S2}x_{S2}^*(1-x_{R2}^*) - \mu_R x_{R2}^* &= 0 \\
\beta_{W2}x_{W2}^*(1-x_{G2}^*) - \mu_G x_{G2}^* + \tilde{b}_G x_{G1}^*\frac{N_{G1}^*}{N_{G2}^*} &= 0 \\
((1-q_W)\beta_G x_{G2}^*\frac{N_{G2}^*}{N_{W2}^*} + \tilde{\beta}_{SW}x_{S2}^*)(1-x_{W2}^*) - \mu_W x_{W2}^* &= 0
\end{aligned} \quad (20)$$

which are identical to the equilibrium conditions (13) for patch 2 alone, in which we have determined that if $R_2 > 1$, either 1 or 3 endemic equilibrium exists, in addition to the disease free equilibrium (which always exists).

If instead, $R_1 > 1$, we assume that x_{G1}^* is the positive equilibrium given in Appendix B for system (6) with $p_W = 0$. Thus, in determining possible endemic equilibrium values for this system, we may solve the 3rd equation of (19) to obtain

$$x_{G2}^* = \frac{\beta_{W2}x_{W2}^* + \tilde{b}_G x_{G1}^* \frac{N_{G1}^*}{N_{G2}^*}}{\beta_{W2}x_{W2}^* + \mu_G} \tag{21}$$

We substitute x_{G2}^* into the 4th equation obtaining

$$\left[\tilde{\beta}_G \left(\frac{\beta_{W2}x_{W2}^* + \tilde{b}_G x_{G1}^* \frac{N_{G1}^*}{N_{G2}^*}}{\beta_{W2}x_{W2}^* + \mu_G} \right) + \tilde{\beta}_{SW} x_{S2}^* \right] (1 - x_{W2}^*) - \mu_W x_{W2}^* = 0$$

and multiplying through by the denominator we obtain

$$- \left(\tilde{\beta}_G \beta_{W2} + \beta_W \mu_W \right) (x_{W2}^*)^2 - \tilde{\beta}_{SW} \beta_{W2} x_{S2}^* (x_{W2}^*)^2 + \left(\tilde{\beta}_{SW} \beta_G - \tilde{\beta}_{SW} \mu_G \right) x_{S2}^* x_{W2}^*$$

$$+ \left(\tilde{\beta}_G \beta_{W2} - \tilde{\beta}_G \tilde{b}_G x_{G1}^* \frac{N_{G1}^*}{N_{G2}^*} - \mu_G \mu_W \right) x_{W2}^* + \tilde{\beta}_{SW} \mu_G x_{S2}^* + \tilde{\beta}_G \tilde{b}_G x_{G1}^* \frac{N_{G1}^*}{N_{G2}^*} = 0,$$

and dividing every term by μ_W, μ_G, the expression becomes

$$- \left(\frac{\tilde{\beta}_G \beta_{W2}}{\mu_G \mu_W} + \frac{\beta_{W2}}{\mu_G} \right) (x_{W2}^*)^2 + \left(\frac{\tilde{\beta}_G \beta_{W2}}{\mu_G \mu_W} - 1 - \frac{\tilde{\beta}_G \bar{b}_G x_{G1}^* \frac{N_{G1}^*}{N_{G2}^*}}{\mu_W \mu_G} \right) x_{W2}^*$$

$$- \left(\frac{\tilde{\beta}_{SW} \beta_{W2}}{\mu_G \mu_W} (x_{W2}^*)^2 - \left(\frac{\tilde{\beta}_{SW} \beta_{W2}}{\mu_G \mu_W} - \frac{\tilde{\beta}_{SW}}{\mu_W} \right) x_{W2}^* - \frac{\tilde{\beta}_{SW}}{\mu_W} \right) x_{S2}^* \tag{22}$$

$$+ \frac{\tilde{\beta}_G \bar{b}_G x_{G1}^* \frac{N_{G1}^*}{N_{G2}^*}}{\mu_W \mu_G} = 0.$$

Applying the same substitutions in Appendix B, where the first two equations of (19) are identical to the first two equations of (13) in Appendix A and letting $X = \frac{\bar{b}_G x_{G1}^* \frac{N_{G1}^*}{N_{G2}^*}}{\mu_G}$, we obtain

$$D(1 - x_{W2}^*)(x_{W2}^* - \frac{1}{E})x_{S2}^* = (F + 1)(x_{W2}^*)^2 - \left(F + \frac{X+1}{E} \right) x_{W2}^* - \frac{X}{E}. \tag{23}$$

Finally, we use (23) and (15) from Appendix A to obtain a polynomial in x_{S2}^*,

$$\begin{aligned} g(x_{S2}^*) = {} & E(F + 1 + Dx_{S2}^*)[A(B+1)x_{S2}^* + (1 - AB)]^2 (x_{S2}^*)^2 - (FX + Dx_{S2}^*) \times \\ & [C(Bx_{S2}^* + 1)(1 - x_{S2}^*)]^2 [1 - EF + FX + (1 - E)Dx_{S2}^*] \times \\ & [A(B+1)x_{S2}^* + (1 - AB)]x_{S2}^* [C(Bx_{S2}^* + 1)(1 - x_{S2}^*)] = 0. \end{aligned}$$

We note that

$$x_{W2}^* = \frac{x_{S2}^* \left[(A+1)x_{S2}^* - A + \frac{1}{B} \right]}{C(1 - x_{S2}^*) \left(x_{S2}^* + \frac{1}{B} \right)}. \tag{24}$$

is positive if and only if

$$x_{S2}^* > \frac{AB - 1}{AB + A},$$

in which case $AB > 1$ for the expression to be positive (biologically significant).

Thus, we determine that $g(0) < 0$, $g(\frac{AB-1}{AB+A}) < 0$ and $g(1) > 0$, so that g has at least one root in $\left(\frac{AB-1}{AB+A}, 1 \right)$.

Appendix D. **Patches 1, 2, and 3, 2 hosts 2 vectors, no VT, unidirectional migration of infected vectors.** To study the existence of endemic equilibria for system (10) in section 3.7, we first determine that

$$N_{S3}^* = K_{S3}\left(1 - \frac{\mu_S - \tilde{b}_S x_{S2}^*}{r_S}\right), \quad N_{S2}^* = K_{S2}\left(1 - \frac{\mu_S + \bar{b}_S x_{S2}^*}{r_S}\right).$$

$$N_{G2}^* = K_{G2}\left(1 - \frac{\mu_G - \tilde{b}_G x_{G1}^*}{r_G}\right), \quad N_{G1}^* = K_{G1}\left(1 - \frac{\mu_G + \bar{b}_G x_{G1}^*}{r_G}\right).$$

The remaining equilibrium conditions are given by

$$
\begin{aligned}
\beta_R x_{R3}^*(1 - x_{S3}^*)N_{S3}^* - \mu_S x_{S3}^* + \tilde{b}_S x_{S2}^* N_{S2}^* &= 0 \\
\beta_S x_{S3}^* N_{S3}^*(1 - x_{R3}^*) - \mu_R x_{R3}^* N_{R3}^* &= 0 \\
((1 - q_S)\beta_R x_{R2}^* + q_S \beta_{WS} x_{W2}^*)(1 - x_{S2}^*)N_{S2}^* - (\mu_S + \bar{b}_S)x_{S2}^* N_{S2}^* &= 0 \\
\beta_{S2} x_{S2}^* N_{S2}^*(1 - x_{R2}^*) - \mu_R x_{R2}^* N_{R2}^* &= 0 \\
\beta_{W2} x_{W2}^*(1 - x_{G2}^*)N_{G2}^* - \mu_G x_{G2}^* N_{G2}^* + \tilde{b}_G x_{G1}^* N_{G1}^* &= 0 \\
((1 - q_W)\beta_G x_{G2}^* N_{G2}^* + q_W \beta_{SW} x_{S2}^* N_{S2}^*)(1 - x_{W2}^*) - \mu_W x_{W2}^* N_{W2}^* &= 0 \\
\beta_W x_{W1}^*(1 - x_{G1}^*)N_{G1}^* - (\mu_G + \bar{b}_G)x_{G1}^* N_{G1}^* &= 0 \\
\beta_G x_{G1}^* N_{G1}^*(1 - x_{W1}^*) - \mu_W x_{W1}^* N_{W1}^* &= 0
\end{aligned}
\tag{25}
$$

If $x_{G1}^* = x_{W1}^* = 0$, the remaining equilibrium conditions are

$$
\begin{aligned}
\beta_R x_{R3}^*(1 - x_{S3}^*)N_{S3}^* - \mu_S x_{S3}^{1} * + \tilde{b}_S x_{S2}^* N_{S2}^* &= 0 \\
\beta_S x_{S3}^* N_{S3}^*(1 - x_{R3}^*) - \mu_R x_{R3}^* N_{R3}^* &= 0 \\
((1 - q_S)\beta_R x_{R2}^* + q_S \beta_{WS} x_{W2}^*)(1 - x_{S2}^*)N_{S2}^* - (\mu_S + \bar{b}_S)x_{S2}^* N_{S2}^* &= 0 \\
\beta_{S2} x_{S2}^* N_{S2}^*(1 - x_{R2}^*) - \mu_R x_{R2}^* N_{R2}^* &= 0 \\
\beta_{W2} x_{W2}^*(1 - x_{G2}^*)N_{G2}^* - \mu_G x_{G2}^* N_{G2}^* &= 0 \\
((1 - q_W)\beta_G x_{G2}^* N_{G2}^* + q_W \beta_{SW} x_{S2}^* N_{S2}^*)(1 - x_{W2}^*) - \mu_W x_{W2}^* N_{W2}^* &= 0
\end{aligned}
\tag{26}
$$

If $R_1 < 1$, $R_2 > 1$, x_{S2}^*, x_{W2}^*, and x_{G2}^* are all positive, then it is clear that $x_{R3}^* = x_{S3}^* = 0$ is not a solution to system (26). Thus, we have existence of 1 or more endemic equilibrium in patches 2 and 3 alone. On the other hand, if x_{G1}^* and x_{W1}^* are positive, then infection must persist in all patches, i.e. $x_{G2}^* = x_{W2}^* = x_{S2}^* = x_{R2}^* = x_{R3}^* = x_{S3}^* = 0$ is not a solution to system (25). Intuition suggests that there exists one endemic equilibria for patch 3 alone if $R_1 < 1$ and $R_2 < 1$. In this case, if we set $I_{S2}^* = I_{R2}^* = I_{W2}^* = I_{G2}^* = 0$, system (10) breaks down to the simple one host one vector model in which there exists precisely one endemic equilibrium if and only if $R_3 > 1$.

E-mail address: britnee@dbu.edu
E-mail address: kribs@uta.edu